Characterization of the surface condition in AA6061 resulting from deep rolling as a function of common industrial parameters

Andrew Kenneth Layer

Recommended Citation

CHARACTERIZATION OF THE SURFACE CONDITION IN AA6061 RESULTING

FROM DEEP ROLLING AS A FUNCTION OF COMMON INDUSTRIAL

PARAMETERS

by

ANDREW KENNETH LAYER

A THESIS

Presented to the Faculty of the Graduate School of the

MISSOURI UNIVERSITY OF SCIENCE AND TECHNOLOGY

In Partial Fulfillment of the Requirements for the Degree

MASTER OF SCIENCE IN MECHANICAL ENGINEERING

2019

Approved by:

Dr. Lokeswarappa R. Dharani, Advisor
Dr. Daniel S. Stutts
Dr. Nicholas N. Nanninga

ABSTRACT

Roller burnishing is widely used in industry to improve the surface finish and fatigue life of components. As weight reduction continues to grow in the automotive and transportation industries, deep rolling can help maintain product performance by mitigating the increase in component stresses resulting from lower weight systems. Deep rolling parameters such as tool, applied angle, feed rate, spindle speeds, and relative tool direction all affect cycle time, product performance, and appearance. The effects of common industrial parameters on the resultant surface roughness and residual stress profiles were studied in this investigation. The samples were manufactured on a CNC lathe using industry standard tooling. Surface roughness was measured by use of a contact profilometer. The components residual stresses were measured using the Hole Drill Method (ASTM E837). The compressive stress magnitudes, depths, and orientation of the residual stress were characterized. The results suggest that the type/mechanism of the burnishing tool was the most statistically significant contributor toward surface roughness and compressive residual stress. Feed rate was the second most significant experimental parameter. Additionally, a correlation between roughness and residual stress was found when using a constant burnishing tool.

ACKNOWLEDGMENTS

I would first like to thank the management team of Accuride for seeing value in this program and for financially supporting this academic endeavor. This research would not have been possible without industry support. In addition, I would like to thank Teah Allen for her help in data collection throughout this project and I hope that this research project boosted her academic progression as well.

From an academic perspective, the support of my advisor Dr. Dharani, the motivation and guidance of Dr. Nanninga, the encouragement of Dr. Kinzel while in my undergraduate, and the firm example of my father Dr. Layer have all shaped my path and I cannot thank this diverse community enough for encouraging my growth in academia.

To my wife Kaleen, the encouragement and patience you have shown me throughout this period has allowed me to complete this work. Without your grace this undertaking would have been impossible.

Lastly, I would like to dedicate this work to James Layer. Although my grandfather will not be able to read this work, as I reflected on his too early loss, I realized that there are parallel themes between grandparents and a thesis. As I read through published literature on my topic to educate myself and find a pathway to broaden the body of knowledge, I realized that grandparents in the same way educate and broaden the base of their children and grandchildren and the value this brings cannot be overlooked.

TABLE OF CONTENTS

Page

LIST OF ILLUSTRATIONS

LIST OF TABLES

NOMENCLATURE

Symbol	Description
DOE	Design of Experiments
EBSD	Electron Backscatter Diffraction
HD	Hole Drill Method (ASTM E837)
RPM	Revolutions per minute. From a CNC perspective contorlled by the use of a G96 code
SEM	Scanning Electron Microscope
SFM	Surface feet per Minute. From a CNC perspective controlled by the use of a G97 code. Maintains a constant linear surface speed by modulating RPM as a funciton of radial tool location
XRD	X-ray diffraction

1. INTRODUCTION

Weight reduction is an important theme of modern mechanical design resulting from a multitude of customer needs and economic or political factors: greenhouse gas emission regulations driving increases in efficiencies, trade wars affecting costing of imported goods or materials, and intracompany cost savings driven by shareholders or financial owners, are several of the key drivers for the automotive industry. From an engineering perspective, a large portion of automotive components are designed for fatigue life rather than static strength with many components being subjected to both contact and non-contact fatigue situations. As these components become lighter while experiencing identical multi-axial fatigue loads as their heavier counterparts, fatigue damage can often increase non-linearly with weight. An unspecified component within the automotive industry observed up to a 25% increase in maximum principle strain after the geometry was changed to save 5% weight during an accelerated fatigue test.

As fatigue sensitive products continue to decrease in weight while maintaining identical in-field loading, changes in design criteria must occur to ensure product reliability. New or enhanced processes must be incorporated into existing manufacturing systems, new materials must be researched and adopted into value streams, and often final product costs cannot increase. The focus of this work is roller burnishing. Application is integration of process design into product design for effective product weight reduction.

1.1. RESIDUAL STRESSES

Significant research into the formation of beneficial compressive residual stresses can be found in the literature. Enhancements in the performance of fatigue sensitive components is well understood. However, the majority of the reviewed literature focuses on 7000 series aluminum based on its prevalence in the aerospace industry [2, 6, 7, 8, 19, 22]. Within the automotive industry, 6000 series alloys are commonly used due to their generally good strength to weight ratio, good corrosion resistance, and ease of manufacturing with respect to forming and machining processes and was the focus of several investigative studies [6, 9, 10] while 2000 series aluminum was the third most common alloy covered in the literature [3, 4, 6, 22]. These predominant aluminum alloys are strengthened through precipitation hardening, whereas 3xxx and 5xxx series aluminum gains strength through solid solution strengthening. Additional material mechanisms that effect material strength are dislocation density and strain rate hardening. These factors all effect the formation of residual stresses within a specific material.

Before an in-depth analysis of residual stress is conducted, a better definition and scope of residual stress is required. In the textbook *Practical Residual Stress Measurement Methods,* Schajer [13] defines three types of residual stress. Type I stresses occur on the macro scale and normally form as a result of mechanical or thermal treatments. Type II stresses occur at the micron scale and are related to grain boundaries while Type III stresses occur at the meso scale affecting material dislocations and crystal interfaces. A majority of the literature focuses on Type I residual stresses as this form of stress is most commonly manipulated to affect positive performance in components. Type I stresses are the focus of this work.

Residual stresses are a function of a material's yield strength. The formation of residual stress results from the elastic relaxation following plastic deformation. Cold working or strain hardening could locally affect near-surface yield strength which can produce more compressive residual stress profiles. Additionally, a compressive residual stress requires a tensile stress at some location in the component to satisfy equilibrium conditions. This work deals with the stress distribution most related to peening shown in Figure 1.1, where a plastic deformation occurring at the product surface results in a sub-surface gradient of compressive residual stress common with Type I stresses.

Loading/Plastic Deformation   Residual Stress Field
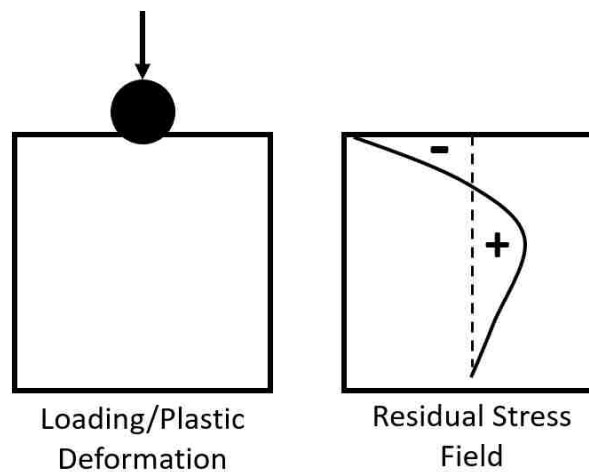
Figure 1.1 Types and Distributions of Residual Stress [13]

Stephens [15] states that "the most widely used mechanical process for producing beneficial compressive surface residual stresses for enhancing long, and intermediate fatigue life are shot-peening and surface rolling." This statement was supported by a study highlighting the effects of compressive residual stresses on a steel bar in three states: smooth, notched, and notched with the surface treated with shot-peening. The

results revealed that compressive residual stresses eliminate the detrimental notch effect on fatigue life when compared to the unnotched specimen.

Mohseni [8] attempts to differentiate the difference between deep rolling and roller burnishing by applying deep rolling to the formation of sub-surface compressive residual stress whereas roller burnishing is a process to induce a fine surface finish or geometric tolerance onto a component. However, this contradicts the industry terminology presented by Beghini [2] with references to Lambda and Ecoroll corporations that have designed and manufactured "low plasticity burnishing elements." This paper will reference burnishing as the processes used to induce sub-surface compressive residual stresses. In addition to shot peening and roller burnishing as previously mentioned, Mohseni [8] also incorporates discussion on laser peening and ultrasonic peening as more advanced methods of creating residual stress while noting their current lack of commercial feasibility for high-volume production.

1.2. FRETTING FATIGUE

Where compressive residual stresses improve the general fatigue life of components subjected to cyclical loading, a more localized phenomenon occurs when two components are in contact under this same cyclical loading. Majzoobi [7] discussed that fretting fatigue could reduce the fatigue life of components up to 76% if not properly mitigated through design and process. There are some conflicting theories regarding the relationship between surface condition and the initiation/propagation of fatigue damage. Majzoobi [7] focuses on the effect of hardness to protect the surface and speculated that a rougher surface could mitigate fretting through two separate mechanisms. First that a

rougher surface decreases the surface area of contact and therefore decreases the statistical probability of a crack forming, and secondly that a rougher surface creates more regions for abraded particles to reside without adding to the abrasive mechanism. Mohseni [8] focused more on the improvement of surface condition through chemical treatments and surface finish. The focus was on decreasing the frictional force that creates lateral loading and the abrasive condition during the micro-movements required for fretting damage to occur. A summary of Mohseni's investigation is shown in Table 1.1 which coincidently supports that deep rolling (burnishing) is one of the better surface treatments from both performance and economic feasibility.

Table 1.1 Overview of Surface Treatments Used to Mitigate Fretting Fatigue Damage [8]

Surface Modification	Decrease Friction	Induce Compressive Stress	Increase Hardness	Increase Surface Roughness	Durability or Adhesion	Cost	Mitigation of Fretting Wear	Mitigation of Fretting Fatigue
Nitriding	↑	↑↑	↑↑	D	↑↑	↑	↑	↑
Electroplating	D	↓↓	↑	D	↓	↑	↑	↓↓
Hard Anodizing	D	↓	↑	D	↑		↑	D
Shot Peening	↓	↑	↑	↑↑		↑↑	↑↑	↑↑
Laser Shock Peening	D	D	D	↑	↓↓	↑	D	↑
Deep Rolling	↑	↑↑	↑	D	↑↑	↑↑	↑	↑↑
IBED Hard Film	↑	↑	↑	↓↓	↑	↓↓	↑↑	↑↑
PVD Coating	↑	D	↑	↓	D	↓	↑	D
D: Depends on Initial Condition ↑: Improves ↑↑: Greatly Improves ↓: Decreases ↓↓: Greatly Decreases								

The body of evidence supports that compressive residual stresses are a common industrial tool utilized to increase fatigue life of components. The residual stress has a depth profile that increases to a maximum compressive residual stress below the material's surface and degrades to a zero or tensile stress state to maintain equilibrium.

Surface treatments also increase the hardness and change the roughness of the surface which combine to improve fretting fatigue resistance.

1.3. PROJECT SCOPE

The objective of this study is to investigate the effect of common manufacturing parameters on surface roughness and the residual stresses within AA6061 during the burnishing process. This includes statistical confidence analysis on the significance of these results. Additionally, the evolution of the surface roughness is investigated to quantify a metric that relates to product appearance. A final goal is to determine if surface roughness can be used to determine the presence of burnishing in an industrial environment. With respect to quality control, the measurement of residual stress is difficult, requiring specialized equipment and personnel, whereas surface roughness is a common industrial measurement.

2. MATERIALS AND METHODOLOGY

2.1. EXPERIMENTAL AND STATISTICAL DESIGN

To best represent selected automotive components while minimizing costs, thick hot rolled plate AA6061 was selected in the form of a 4'x8'x1" sheet. This raw material, which was heat treated to the T6 condition, was processed on a water jet to produce the multiple geometries of blanks shown in Figure 2.1. The primary specimens were a circular 6.5" diameter puck with two different secondary material characterization samples: chemical/grain size specimens were 3"x3" squares, and tensile blanks were 1"x1"x6".   The material characterization samples were taken at the front, middle, and back of the plate in the transverse and longitudinal directions to obtain baseline material properties and to investigate material anisotropy, as these could affect the characterization analysis of residual stress if significant differences were present.
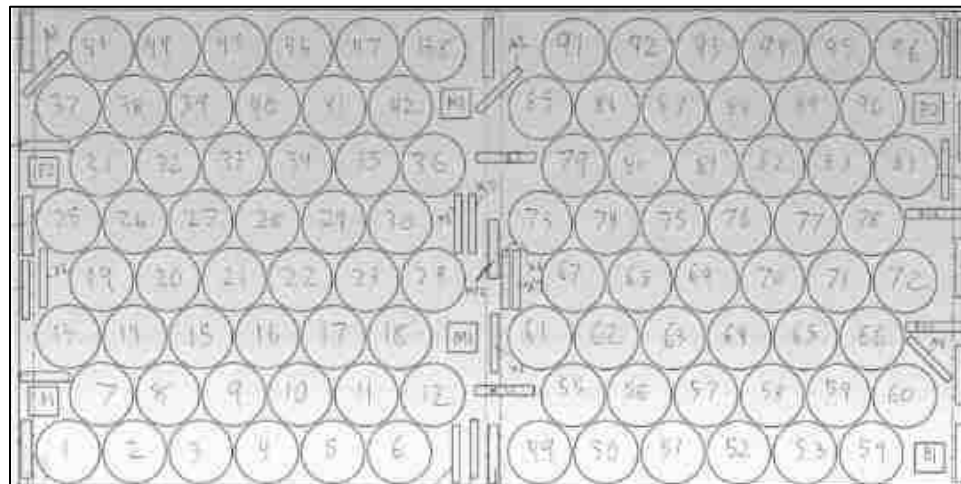
Figure 2.1 Sample Layout and Identification of the Raw Material Samples

The statistical design followed a multi-step confirmation design of experiments (DOE) that limited the number of baseline experiments to a feasible level. There were six experimental variables controlled within this project: burnishing tool, burnishing force, tool angle, tool feed rate, CNC control methodology, and relative direction. Additionally, there were two global response variables: surface roughness and residual stress. Residual stress was further resolved into specific attributes: surface level residual stress, sub-surface depth at which maximum compression stresses occurred, magnitude of maximum compressive stress (minimum principle stress), magnitude of maximum compressive stress at a specific depth, angle of principle stress, and the full width half maximum parameter from x-ray diffraction (XRD) analysis.

The levels of the experimental variables are shown in Table 2.1. Following an unbiased full factorial design, over 250 samples would have been required to complete the mathematical array. Instead, a baseline assumption was that the behavior of each tool would be similar, so that the trends observed for Tool A would be valid Tool B. Additionally, it was assumed that within the levels selected, there were negligible interaction affects between the two groups of variables tested in each DOE, therefore the results could be combined using superposition to make global assumptions.

The first DOE only modulated the experimental variables of burnishing tool, force, and angle, while maintaining the other three variables at a constant 0.020"/rev feed rate and pushing the material at a constant RPM of 1,000. The second DOE modulated feed rate, direction, and control method while maintaining the other three variables at a constant 205 lbs. force at 15° angle using a constant burnishing tool (EG5 – 3.0" roller).

This resulted in approximately 60 samples to cover the range of responses created by each unique tool.

Table 2.1 Experimental Variables

Burnishing Tool	Burnishing Force (lbs.)	Burnishing Angle (°)	Feed Rate (in/rev)	Direction	Control Method
HG 13	115	0	0.005	Push	RPM – 500
HG 25	160	15	0.010	Pull	RPM – 1,000
EG 5 – 3.0"	205	30	0.015		SFM – 675
EG 5 – 5.5"			0.020		SFM – 1,350

Due to the number of variables being affected within this experiment, a method of randomization was planned to minimize the effect of systemic error across the design. Using the identification in Figure 2.1, the samples were randomly selected from the geometry of the raw material to minimize any effect of material anisotropy throughout the plate. Likewise, during the measurements, samples were randomly analyzed to prevent systemic error. Burnishing order was not able to be randomized due to cost constraints. No form of blocking was included in the design as the same lathe, tools, and operator were used to produce the samples. The repeatability of the CNC lathe and the skill of the operator were assumed sufficient to prevent time-based differences during production.

2.2. EXPERIMENTAL VARIABLES

Four separate tools, all purchased from Ecoroll Corp, were used within the procedure: two mechanical rollers and two spherical hydrostatic tools. The mechanical rollers were an EG5 body with 40M style roller. Both 3.0" and 5.5" diameter rollers with a minor radius of 0.1875" were examined. The hydrostatic tools were an HG13-9E270 multi-angled tool using both an HG13 and HG25 head element. In the mechanical tools, burnishing force was actuated by a spring pack built within the tool body. Each tool was provided with a calibration graph to determine force as a function of displacement using the tools indicator as shown in Figure 2.2. In the hydrostatic tools, there is a linear correlation between pump pressure and burnishing force. The HG13 and HG25 elements used in this experiment use the same hydraulic element and therefore used the same force vs. pressure curve as shown in Figure 2.3. An overview of each tool at the experimental angles is shown in Figure 2.4.
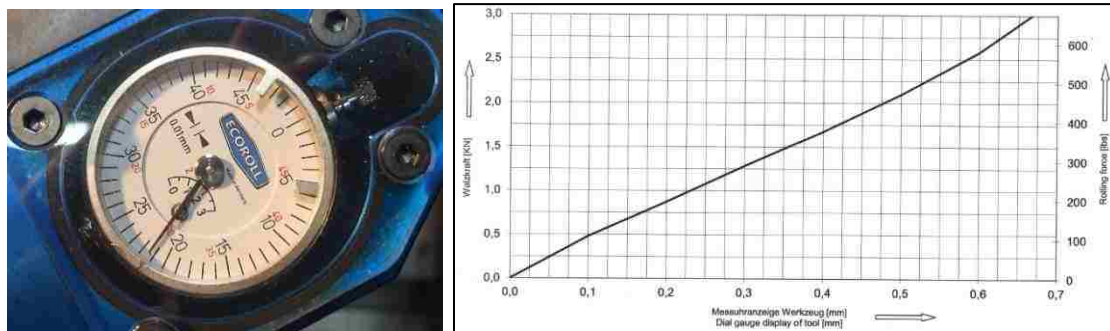
Figure 2.2 Ecoroll EG5 Gauge and Force Calibration Curve
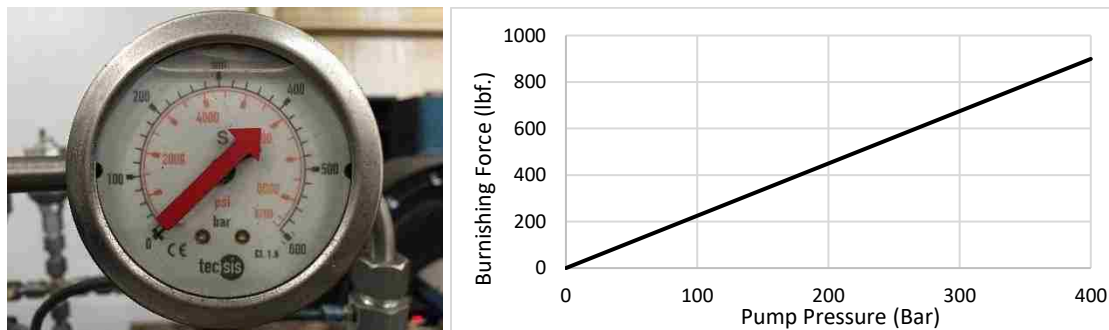
Figure 2.3 Ecoroll Hydraulic Unit Gage and Force Calibration Curve
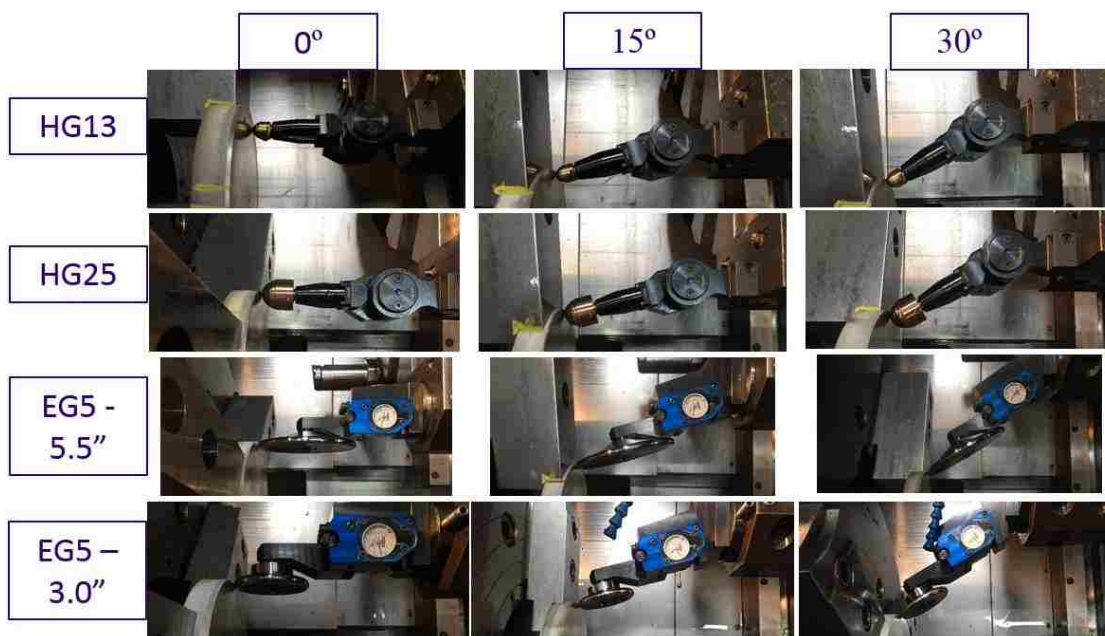
Figure 2.4 Visualization of Burnishing Tools and Angles Utilized during the Manufacturing of Samples

Tool angle was determined either by an adjustable tool body (HG13-9E270) or by physical angular offsets required by the EG5 tool body (Figure 2.4). Feed rate was controlled by a constant inch per revolutions for all experiments, with the magnitude of the feed rate changing per design group. The experimental variable Control was a function of two separate CNC parameters; G96 code for constant surface speed control

using surface feet per minute (SFM) or G97 to cancel SFM control and use revolutions

per minute (RPM). Industry guidelines from Ecoroll Corp recommend SFM control

while using burnishing tools to ensure consistent tool angular velocity while previous

experience with industry burnishing supported use of RPM control. The magnitude was

unique for each control group, with RPM control using parameters of either 500 or 1,000

while SFM using parameters of either 675 or 1300 ft/min based on industry guidelines.

Tool direction is a parameter not controlled by CNC code or industry guidelines.

It is a relationship between the vector of force application and velocity vector of the

burnishing tool. If the applied force and velocity vectors are aligned, the term "pushing"

was used to describe the relative motion. Whereas if these vectors are counter to each

other, the tool's relative motion was described as "pulling". If the burnishing tool was

normal to the surface, no distinction was made. These relative directions are visualized

in Figure 2.5.

Mahajan, et al [6] conducted a thorough literature review relating to the analysis

of burnishing parameters and presented a graphical conclusion relating to the frequency

of these parameters as shown in Figure 2.6.When looking at the depth of these studies, it

was discovered that usually only two or three parameters were tested in a single study

which limits the amount of interaction conclusions that could be determined. This study

includes analysis of initial roughness which was reviewed in seven percent of Mahajan's

study [6] (7%), direction of burnishing (7%), tool angle (not listed), which when

combined with the common force (80%), feed rate (80%), speed (80%) should give a

more comprehensive view not just of specific parameters but also on their interactions if

present. Table 2.2 relates the parameters discussed in Mahajan's et al [6] to the

parameters used in this study.
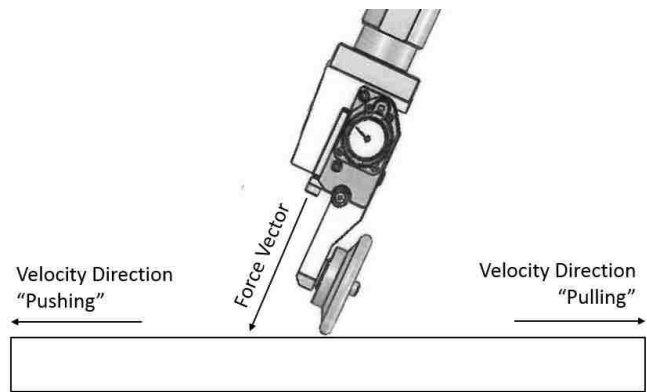
Figure 2.5 Visualization of Relative Tool Direction
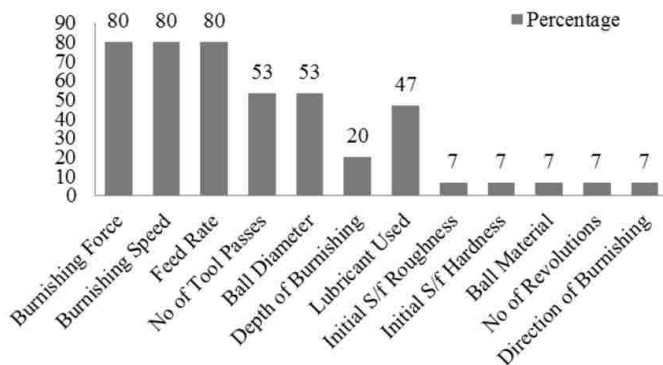
Figure 2.6 Frequency of Burnishing Parameters in Current Literature [6]

2.3. RESPONSE VARIABLES

There are three primary groups of response variables within this project: surface

roughness, Hole Drill (HD) residual stress, and XRD residual stress results. XRD and

HD were selected as a function of availability and cost as shown in Figure 2.7.

The surface roughness results were measured using four separate parameters to ensure at least a single parameter could isolate changes due to the experimental variables. Ra is the arithmetic mean of the roughness profile, Rz is the average distance between the maximum and minimum peaks, Rt is the maximum height of the profile, and Rsm is the average peak to peak distance. All four parameters were calculated from a single measurement pass of the surface profilometer

Table 2.2 Current Study Compared to Current Literature Review by Mahajan [6]

Study Variable	Literature Review Variable	Literature Review Frequency
Burnishing Tool	Ball diameter	53%
Burnishing Force	Burnishing Force	80%
Tool Angle	N/A	0%
Feed Rate	Feed Rate	80%
Direction	Direction of Burnishing	7%
Control Method	Burnishing Speed	80%

XRD utilizes the measurement of crystal distortion resulting from the presence of elastic residual stresses, as highlighted in Figure 2.8. XRD is a function of spacing between lattice planes (d), Braggs angle (°), and the selected wavelength of the radiation (λ) [13]. XRD has the benefits of being truly non-destructive, high resolution, and measures the near surface stresses better than HD due to the limited penetration depth of X-rays compared to the large-scale removal (relative) required for HD.

As few crystals are perfect, the diffraction pattern will exhibit a range of results creating a histogram of counts vs. angle. The location of the peak or shift from the nominal position is used to measure the residual stress while the width of the peak produces what is referred to as the full width half maximum (FWHM) parameter shown in Figure 2.9. FWHM can be used to indicate the amount of localized hardening on the surface due to an increase in dislocations where a larger value indicates a greater presence of material dislocations and a higher surface hardness (cold working).
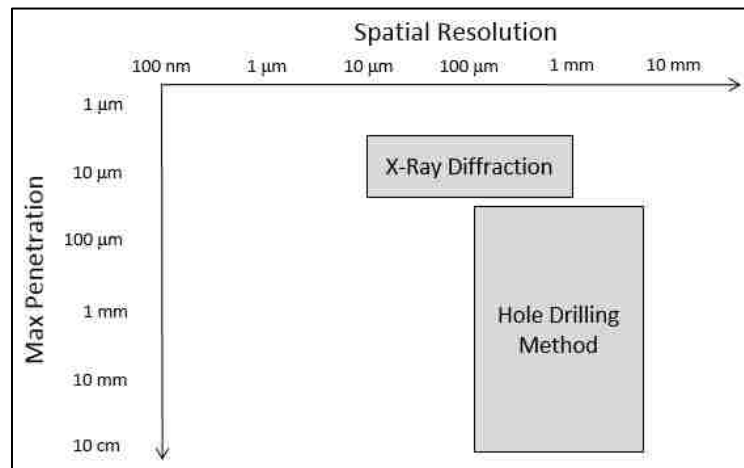
Figure 2.7 Residual Stress Summary Regarding Penetration and Resolution [13]
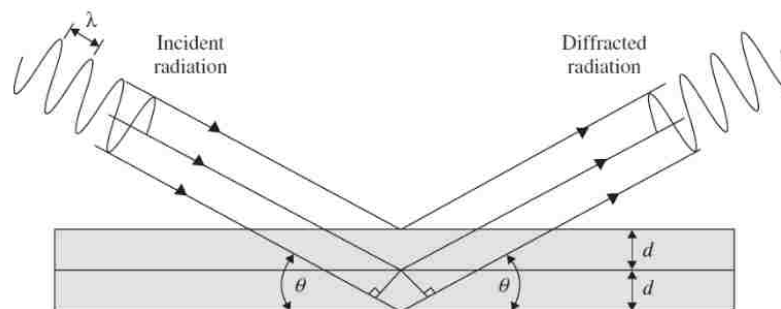
Figure 2.8 X-Ray Diffraction Illustration [13]

Although XRD can be used to generate depth profiles of residual stress, electropolishing or advanced high-speed machining is required to ensure no additional stresses are generated in the material. These processes significantly increase the time, and complexity when using XRD when compared to the Hole Drill method. Therefore, the hole drill method was selected as the primary method to generate residual stress vs. depth data when combined with the Integral Method discussed in ASTM E837. Figure 2.10 highlights a general residual stress vs. depth generated using the Integral Method (H-Drill software).
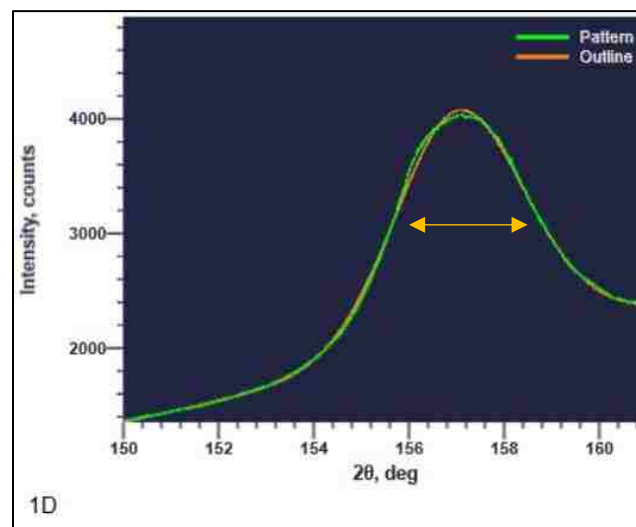
Figure 2.9 XRD Full Width Half Maximum Visualization

Surface level residual stress can be difficult to accurately measure with HD due to the large gradients and near surface effects of the measurement process (XRD is usually the preferred method) and often shows few conclusive results. Additionally, the deeper sub-surface stresses can be difficult to accurately measure due to measurement system

limitations. When accounting for standard strain error, depth and hole diameter measurement variation, along with material property variation, HD residual stress measurements can include a confidence bound as shown in Figure 2.10. At depths greater than 0.031, the error bounds exponentially increase, decreasing the confidence of results. The depth of 0.031" was selected as cutoff for reliable measurements within this project.
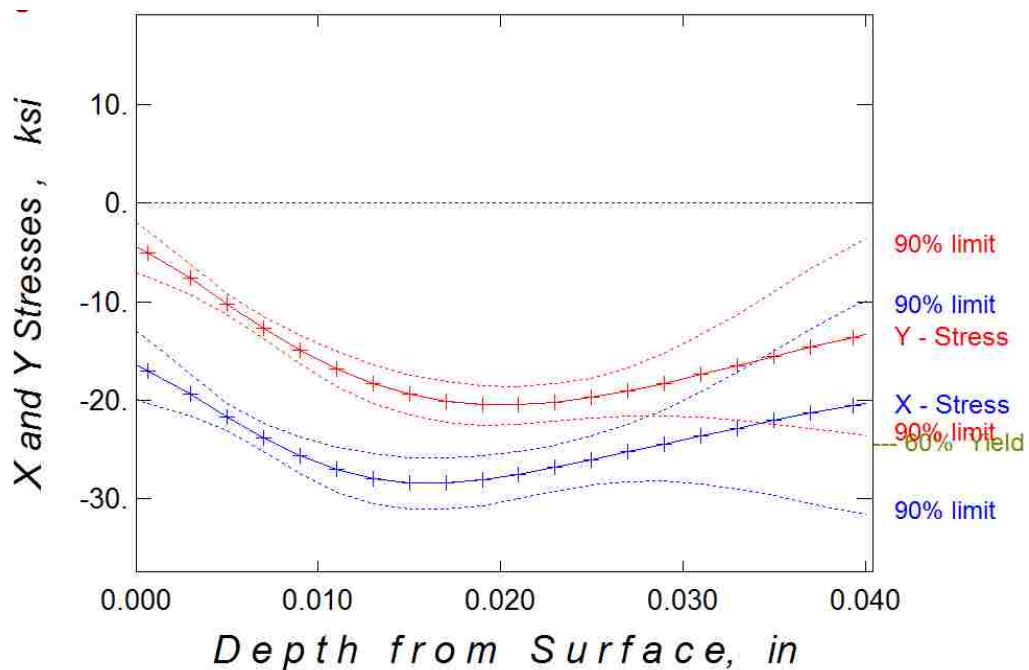
Figure 2.10 Integral Method – Residual Stress vs. Depth

2.4. MANUFACTURING PROCEDURES

The 6.5" diameter pucks and all secondary characterization samples were water jet from the sheet of 6061 aluminum and scribed with the sample ID's shown in Figure 2.1. The circular pucks were randomly pulled from the population and machined/burnished in back to back operations without removing the puck from the lathe

chucks. This was done to minimize the effect on non-uniformity on the burnishing operation. The machining process was completed with a 12mm button insert (Sandvik RCGx 12 01 MO-AL), a single roughing pass with parameters of 1,400 RPM's, 0.04"/revolution feed rate and 0.08" depth of cut, and a single finishing pass with parameters of 1,400 RPM's, 0.018"/revolution feed rate and 0.045" depth of cut. These lathe parameters were chosen in order to induce tensile residual stresses produced by a subtractive manufacturing process.

Where machining of the surface layer was easily repeated using a standard G code, each burnishing operator required at least a touch-off confirmation before burnishing was completed. For the hydrostatic tools, the tool was touched off at max extension, and with pressure removed, the tool's offset was set to one half of the burnishing tool's stroke. For the mechanical tool, the tool was manually adjusted until the spring pack dial read the desired value 50 RPM. The CNC program was then run to process the surface. Any variation in actual applied force resulting from the setup or dynamic effects was assumed constant between groups and would mirror industry conditions.

After each sample was machined and burnished, the puck was removed from the lathe, inspected for obvious damage, cleaned with an industrial degreaser, and packaged with foam to prevent surface damage during transport between the manufacturing facility and laboratory.

2.5. MEASUREMENT SYSTEMS AND PROCEDURES

There were five separate material characterizations that were completed in this project. Material hardness was measured using a standard Brinell hardness test using a 10mm tungsten carbide indenter with a 500kg load for 30 seconds following ASTM E10-18. Tensile tests were conducted following ASTM E8/E8M-16a with strain rate control with a 30-kip load cell. Initial grain structure was imaged using Kellers etchant and optical microscopy. Quantitative analysis of grain size was completed on a Zeiss SEM utilizing an EDAX EBSD to measure grain size.
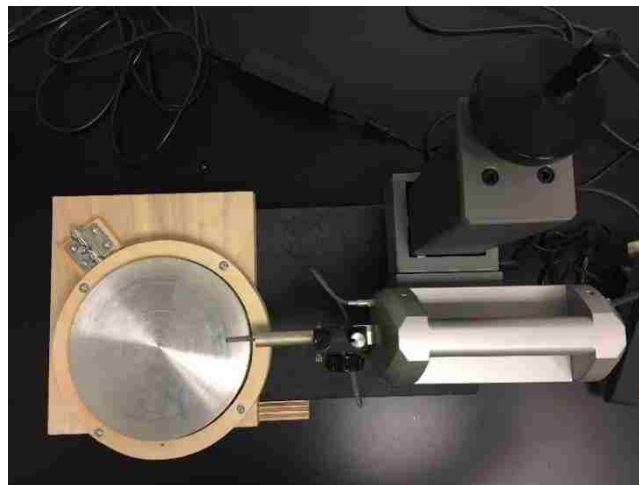
Figure 2.11 Surfcom E50 with Fixture for Repeatable Surface Roughness Measurements

The surface roughness was measured using a Surfcom E50 profilometer calibrated to ISO1997/2009 standards. An evaluation length of 0.1575" was used with 5 sub-lengths and a measurement speed of 0.012"/sec. A fixture was constructed to ensure consistency of measurements with four radial measurements taken per sample (90 degrees apart). Figure 2.11 shows the fixture used to complete the measurements. The

average radial location of roughness measurements was 2.4" from center of specimen.

Residual stresses were initially measured using XRD utilizing a Rigaku system. The

device used a Chromium radiation source, Kα1 and Kα2 waves, a 2mm collimator, and a

60 second exposure time. The sample was aligned with the beam angle hitting radially at

a location 2.4" from specimen center.

Residual stress was primarily measured using the hole drill method following

ASTM E837. Vishay 062UL rosette strain gages were used with a HBM MX1615B

controller/conditioner and Catman easy analysis software. The strain gages were

installed with Gage 1 aligned in the radial direction away from the specimen center to

allow consistent comparisons regarding principle stress directions following the

mathematical nomenclature presented in Vishay's Tech Note 503 [17] (Figure 2.12).
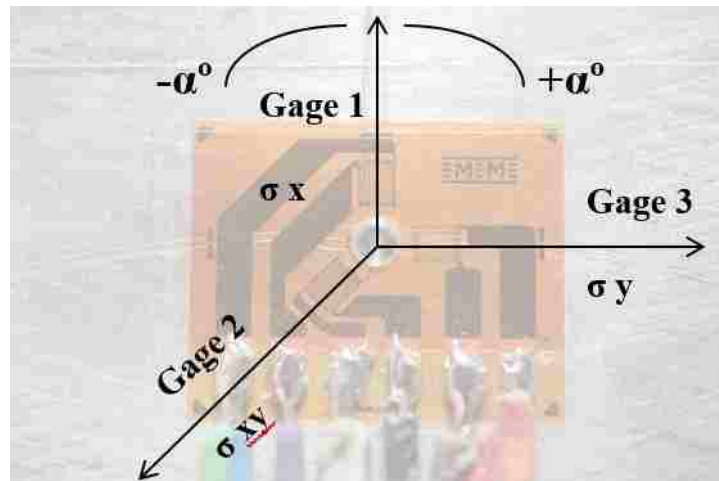
Figure 2.12 Hole Drill Stress Orientations and Nomenclature

The strain gage location was controlled with a marking fixture (Figure 2.13) to

ensure strain measurements occurred 2.4" radially from specimen center while

maintaining proper alignment. This was done to ensure roughness and residual stress measurements were measured at the same location. The burnished samples were clamped into a fixture that constrained the Vishay hole drill device onto the sample and the sample to the fixture base as shown in Figure 2.14.
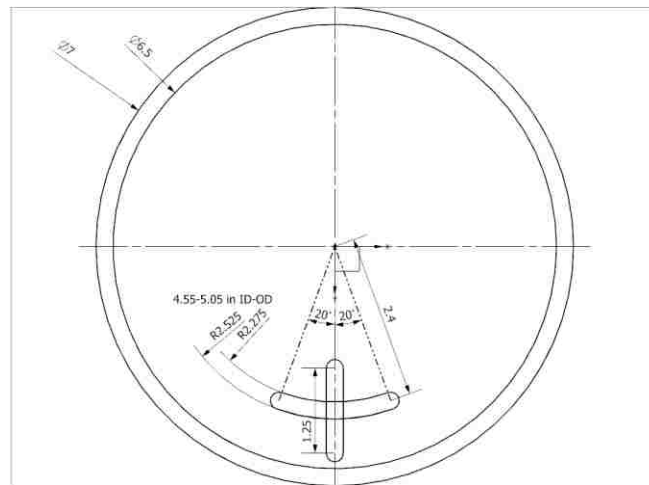
Figure 2.13 Strain Gage Alignment Fixture

Figure 2.14 Hole Drill Fixture

The HD process utilized a high-speed pneumatic mill using a carbide cutter with proper edge relief and 0.05" diameter to align with the best practices described by Schajer [14]. Additionally, the mill's spindle was offset to create ~0.012" runout to produce an average hole diameter of 0.085" with a maximum hole depth of 0.04" again following the recommended practice of Schajer [14]. Strain measurements were recorded at increments of 0.002" with a 0.0005" drill increment per step while rotating the drill a full 360° for each step increment to ensure a clean, circular hole as shown in Figure 2.15.
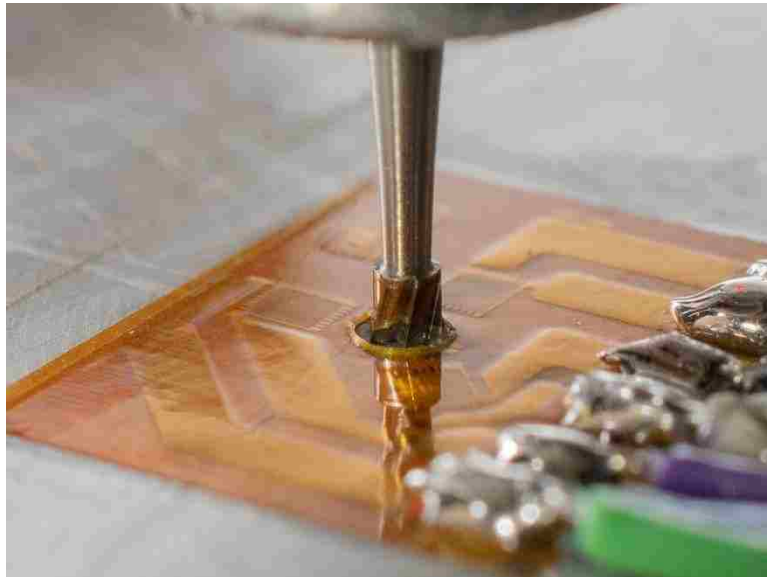
Figure 2.15 Hole Drill Technique [14]

Additionally, the strain measurements were taken with a 2.5V excitation voltage following guidance in Vishay's TN502 [16] in order to maximize the resolution of the system. With an excitation voltage of 1V, the system reported a maximum resolution of 20 mV/V through the HBM MX1615B but had a system resolution of 8 mV/V with an excitation voltage of 2.5V.

This was the maximum value allowed without risking thermal creep in the strain gage [16]. The HBM system utilized an averaged strain measurement taken at 10 Hz for 10 seconds to minimize the noise error with a manual trigger for collection. Hole dimensions were measured using an optical microscope and Nikon image analysis software, with both height, width, and 8-point average diameter results being recorded and averaged as shown in Figure 2.16. The HD fixture shown in Figure 2.14 prevented invalid milling results (Figure 2.16a) characterized by holes with diameters larger than 0.1" or uneven material removal: Figure 2.16b highlights a valid hole for the HD method. Residual stress measurements were calculated using the software "H-drill" using the procedural step depths, measured hole diameter, proper gage selection, and the recorded strain results as the system inputs
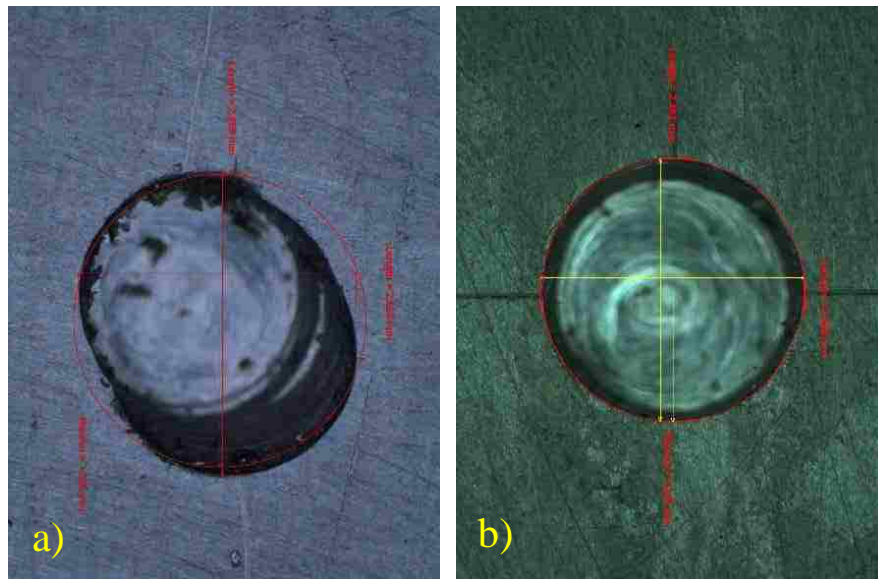
Figure 2.16 Example of Hole Measurements Utilizing Nikon Image Analysis Software a) Invalid Hole Due to Non-Circularity b) Valid Hole with Acceptable Geometric Properties

3. RESULTS AND DISCUSSIONS

3.1. MECHANICAL PROPERTIES

Before surface roughness or residual stress could be measured/discussed, the

material properties were determined in order to support down-steam analysis. Burnishing

is a plastic deformation operation and "a clear consequence of this very limited work

hardening is that the initial yield strength limits the maximum residual stress any

mechanical treatment can induce" Benghini [2]. As stated in the methodology section,

tensile coupons were tested following ASTM E8/E8M-16a guidelines with samples taken

parallel, perpendicular, and 45° offset from the rolling direction with the intent on

characterizing material anisotropy. The results (average of two samples) are provided in

Table 3.1.

Table 3.1 Material Yield Strength

Yield Strength (ksi)			
	Lateral	Transverse	45°
Front	39.4	42.3	39.4
Middle	39.8	41.7	39.1
Back	38.5	41.8	38.7

Based on the relationship between the yield strength and maximum possible

residual stress, the yield strength was determined to be the primary control variable of

interest when compared to ultimate strength and percent elongation. The unaveraged

tensile test results were used in a general linear ANOVA model to determine if there

were significant differences between the location and direction. The ANOVA model

shown in Figure 3.1 used a confidence interval of 0.05 and interaction between location

and orientation was included. Shown in Figure 3.2 is the ANOVA main effects plot for

yield strength and Figure 3.3 is the Tukey comparisons to determine statistical

differences/grouping.

```
Analysis of Variance

Source             DF  Seq SS  Contribution  Adj SS   Adj MS  F-Value  P-Value
  Direction         2  35.094        69.52%  36.422  18.2109    20.13    0.000
  Location          2   1.577         3.12%   1.209   0.6047     0.67    0.529
  Direction*Location 4  2.051         4.06%   2.051   0.5128     0.57    0.691
Error              13  11.762        23.30%  11.762   0.9048
Total              21  50.484       100.00%
```

Figure 3.1 ANOVA Results for Material Yield Strength
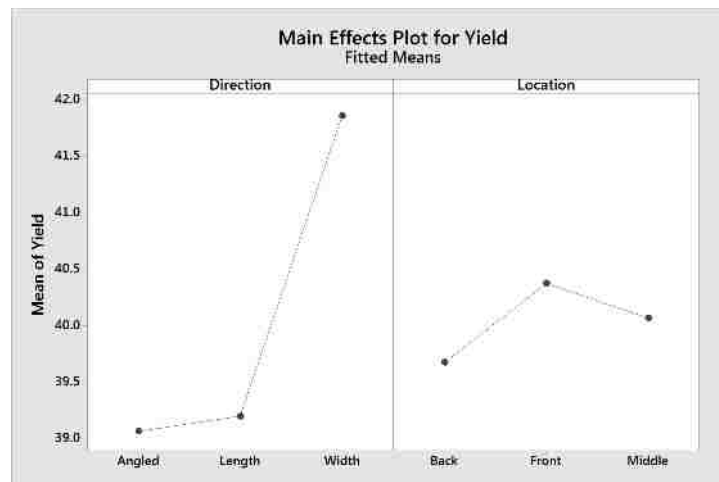
Figure 3.2 ANOVA Main Effects Plot for Material Yield Strength

The ANOVA results support that the direction of the tensile sample with respect

to the rolling direction of the plate was significant whereas the effect of location was not

significant. Using the Tukey comparisons, it can be inferred that samples taken from the

width of the sample were 2.5 ksi higher in yield than both the length or 45° angular offset

samples. From a practical perspective, this material anisotropy was viewed as non-significant as this is a 7% difference in yield strength and the effect of this difference on the hole drill method's analysis was deemed negligible within the 10-30% error band that is standard for the HD method [13]. The average yield strength of the population was 40.7 ksi, with this value being used as a control parameter in the H-drill program.

a)

Direction	N	Mean	Grouping
Width	13	41.8603	A
Length	6	39.2000	B
Angled	3	39.0667	B

b)

Location	N	Mean	Grouping
Front	6	40.3778	A
Middle	10	40.0714	A
Back	6	39.6778	A

Figure 3.3 Tukey Results for Yield Strength a) Direction b) Location

The Brinell surface hardness measurements are recorded in Table 3.2. Each result is an average of three separate measurements taken using the prescribed procedure.

Table 3.2 Material Hardness (Brinell)

	Location 1	Location 2
Front	95.4	98.3
Middle	93.7	89.8
Back	95.2	88.9

Following as similar analysis procedure to Yield Strength, a general linear ANOVA model was used to determine if there was a significant difference in hardness with respect to location. Using a confidence interval of 0.05, the ANOVA results are shown in Figure 3.4 and the Tukey comparison is shown in Figure 3.5. Both support that there is no significant difference in hardness as a function of location, although the

average Brinell hardness was approximately 4.7 higher in the front than the other

locations.

```
Analysis of Variance

Source       DF  Seq SS  Contribution  Adj SS  Adj MS  F-Value  P-Value
   Location   2   97.03        25.30%   97.03   48.51     2.54    0.112
Error        15  286.56        74.70%  286.56   19.10
Total        17  383.58       100.00%
```

Figure 3.4 ANOVA Results for Material Hardness

```
Location  N      Mean  Grouping
F         6   96.8333  A
B         6   92.0833  A
M         6   91.7500  A
```

Figure 3.5 Tukey Plot for Hardness

Grain size characterization was completed using two separate analysis techniques:

optical imaging of the etched grains and quantitative EBSD analysis. The grain size was

initially observed through acidic etching shown in the optical image, Figure 3.6, at two

separate objective magnifications.

The original intent was an optical comparison of grain size to justify the use of

XRD to measure surface residual stresses, orientation, and FWHM results between

known industry samples and the samples covered in this work. Based on the optical

comparison, surface grain structure was of a fine enough scale to allow XRD and

suggested no additional errors resulting from incorrect gain size (where too large of grain

size could result in erroneous XRD results from low signal levels).
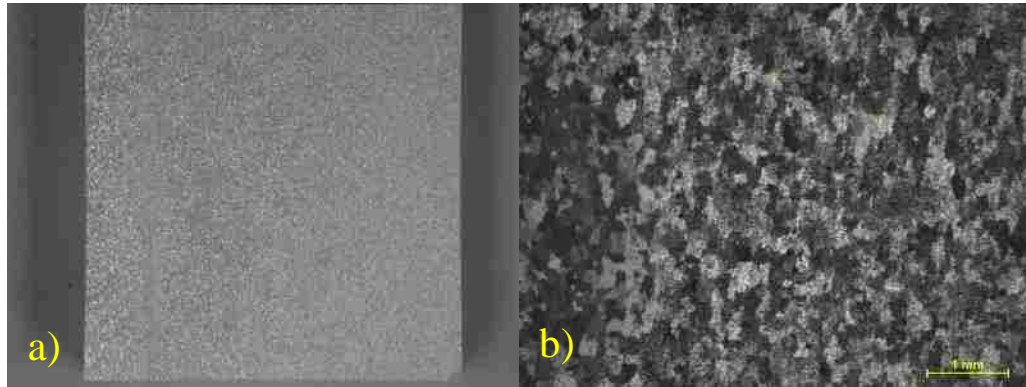
Figure 3.6 Optical Imagery of Etched AA6061 a) 0.67x Objective b) 4.0x Objective

In order to quantify the material grain size, an EDAX EBSD was utilized to characterize the grain sizes and textures along all three dimensions as visualized in Figure 3.7.
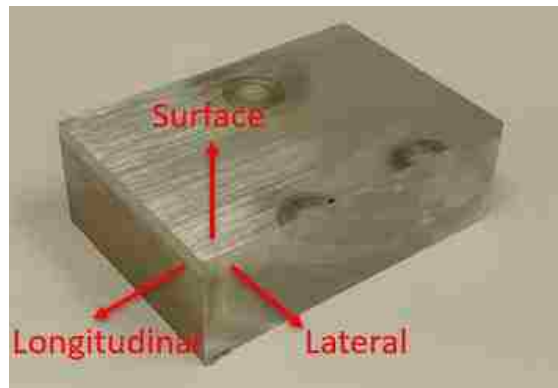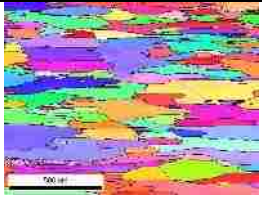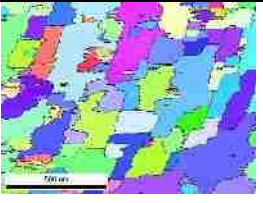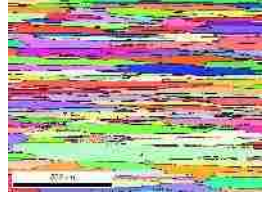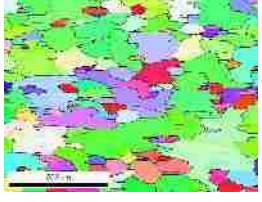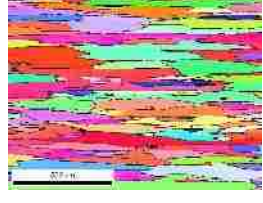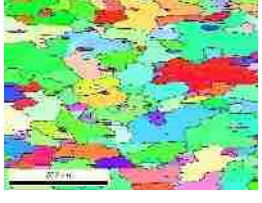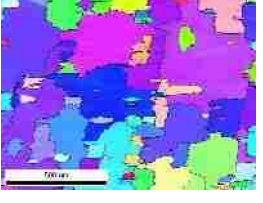
Figure 3.7 Diagram of Grain Size Orientations

Table 3.3 contains the EBSD images of all three orientations at the front (F1), Middle (M1) and Back (B1) locations within the plate of material. It is apparent that the surface has a significantly finer and more elongated structure than compared to the inner structure of the material regardless of orientation. This fine-grained surface was

observed during the initial etching of the material shown previously in Figure 3.6 and

was used to support the use of XRD. The EBSD images of the material cross section

highlights the difference of grain size between the material's surface and core supported

by the grain sizes recorded in Table 3.4.

Table 3.3 EBSD Images of Material Cross Sections

	Surface	Longitudinal	Lateral
F1			
M1			
B1			

To confirm the presence of a near surface gradient of elongated surface grains, an

optical micrograph was taken of the lateral sections surface chemically treated with

Keller's etchant to distinguish the grain boundaries. The result shown in Figure 3.8

supports that a layer of fine grains exists on the rolled surface of the material roughly

0.001" in depth. This material layer would be removed prior to burnishing as 0.125" of

material was removed during the facing operation following the experimental procedure. This would result in the coarse grains being exposed and subsequently burnished which would result in erroneous XRD measurements as general experimental guidelines suggest a grain size between 10µm and 100µm to ensure a proper distribution of x-ray saturation across a surface.

Table 3.4 Average Electron Backscatter Diffraction Analysis: Grain Size Measurements (µm)

	Surface	Longitude	Lateral
F1	96.4	164.8	194.5
M1	141.5	157.9	160.6
B1	160.6	154.4	268.1
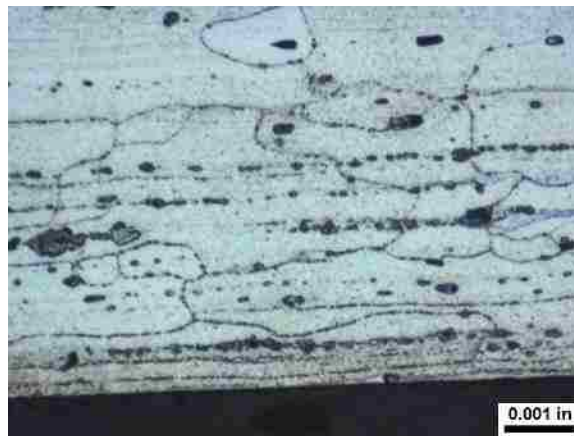
Figure 3.8 Optical Micrograph of Near Surface Microstructure (10x objective)

3.2. XRD MEASUREMENTS

The residual stress results were initially attempted using x-ray diffraction however the results were not conclusive and exhibited poor diffraction results. Shown in Figure

3.9, the differences between a valid and invalid 2θ diffraction histogram curve is visualized. The valid results are characterized by a clear diffraction circle and a distinct histogram and result from a uniform signal. Improper measurements are characterized by discrete diffraction curves and a non-distinct histogram peak.
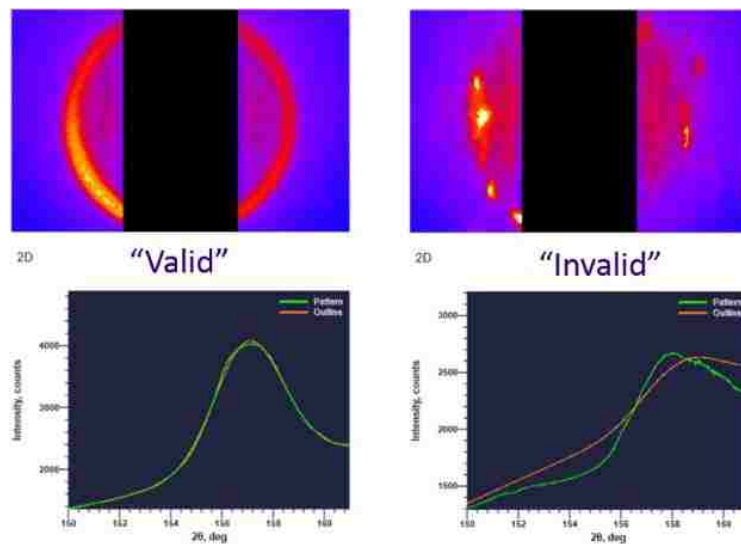
Figure 3.9 Comparison of X-Ray Diffraction Results with Respect to Diffraction Ring and 2θ Histogram Results

3.3. SURFACE ROUGHNESS

As stated previously, there were four common parameters used to quantify surface roughness within industry: Ra, Rz, Rt, and Rsm. Instead of tracking and analyzing all four parameters throughout this project, a sub-section of DOE 1 was selected early in the project and a general linear ANOVA was used to investigate which parameter could best detect a significant difference between groups when force and angle where used as experimental factors while maintaining the same tool (EG5-40M 3.0" roller). The results are shown in Table 3.5, when using a confidence interval of 0.05. Only the roughness

parameter Ra was able to determine significant differences between the groups. This

supported the decision that all remaining analysis would use Ra as the primary response

variable. This is consistent with Ra being the most common roughness parameter in

industrial practice.

Table 3.5 Surface Roughness Significance Results (ANOVA)

	p-values (α=0.05)			
	Ra	Rz	Rt	Rsm
Force	0.003	0.043	0.121	0.860
Angle	0.000	0.089	0.445	0.388
Interaction	0.068	0.456	0.523	0.839
R^2 (adj)	81.30%	40.38%	13.29%	0.00%

Once Ra was determined to be the primary response variable within this project,

the initial surface roughness was characterized. Current literature reports that the initial

surface finish has some level of impact on the post-burnish state [2, 6]. To determine if

the parameters utilized in this work followed a similar trend, the surface finish was

measured in the as-machined state and after burnishing was completed. The results for

every roughness measurement for a specific tool are shown in Figure 3.10 (EG5-40M

3.0") and 3.11 (HG25). The averaged as-machined roughness was approximately 45 μin

Ra. However, buildup of aluminum on the cutter surface could result in excessive

roughness due to poor shearing conditions. To prevent this surface degradation, the

circular carbide insert was rotated every two to four samples. The above average

roughness visible in Figure 3.10 is a result of aluminum buildup that occurred when the

insert was not rotated properly. Each group contains 24 data points, with 4 measurements taken on 6 uniquely processed samples as outlined in Appendix A.
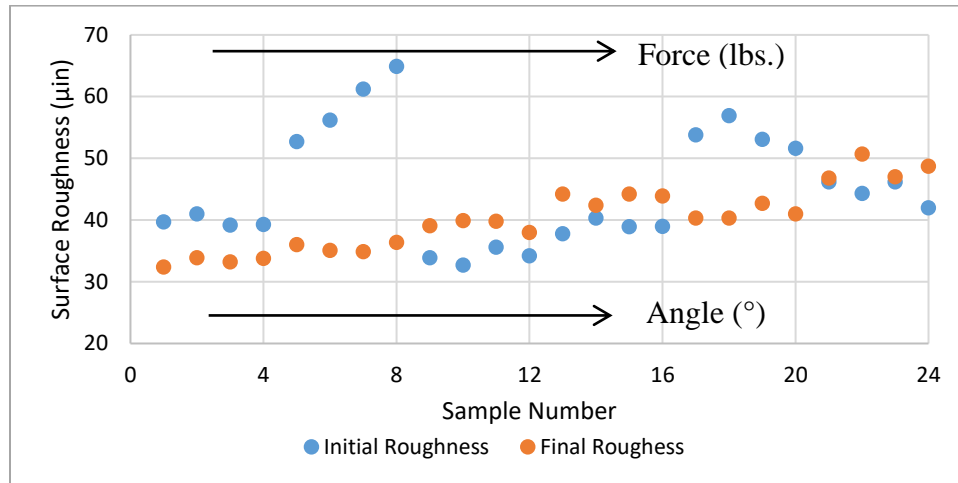
Figure 3.10 Pre/Post Burnishing Surface Roughness (EG5-3.0")

In Figure 3.10, there is a noticeable and consistent increase in roughness as burnishing force and tool angle increase while in Figure 3.11 there appears to be no increase in post-burnishing roughness as a function of force and angle. The consistency of this response could support that there is little effect of the initial surface roughness on the post-burnished condition. To quantify the interaction, the change in roughness was related to the as-machined surface roughness. It was found that for the EG5-40M 3.0" roller (Figure 3.12), when the as-machined surface roughness was less than 45 μin the effect of burnishing resulted in a static increase approximately 5 μin in magnitude. This contrasts with the response if the as-machined surface roughness were greater than 45 μin, where the as-burnished surface shows a greater improvement in roughness. Two conclusions are drawn from this; for the EG5-40M 3.0" roller at a specific machine

parameter (Feed rate, RPM/SFM, Direction), the effects of angle and force result in an

average roughness of ~ 45 μin.
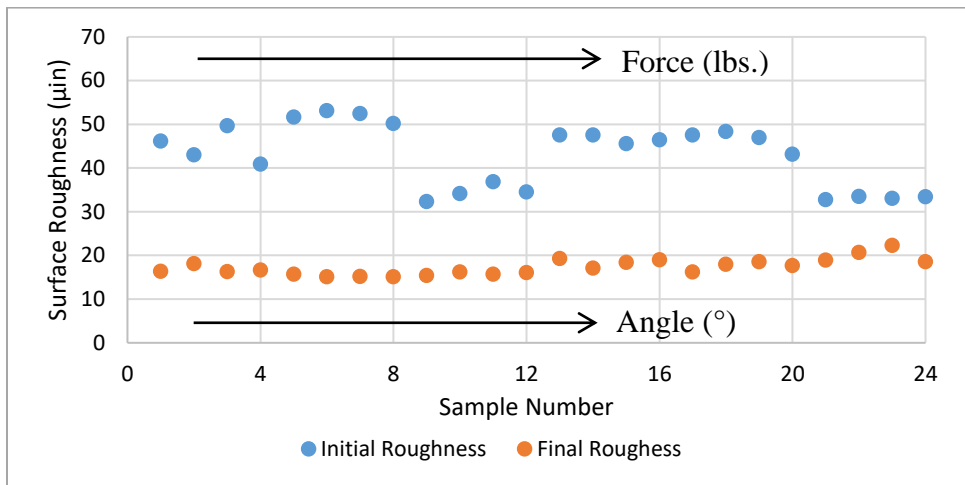
Figure 3.11 Pre/Post Burnishing Surface Roughness (HG25)
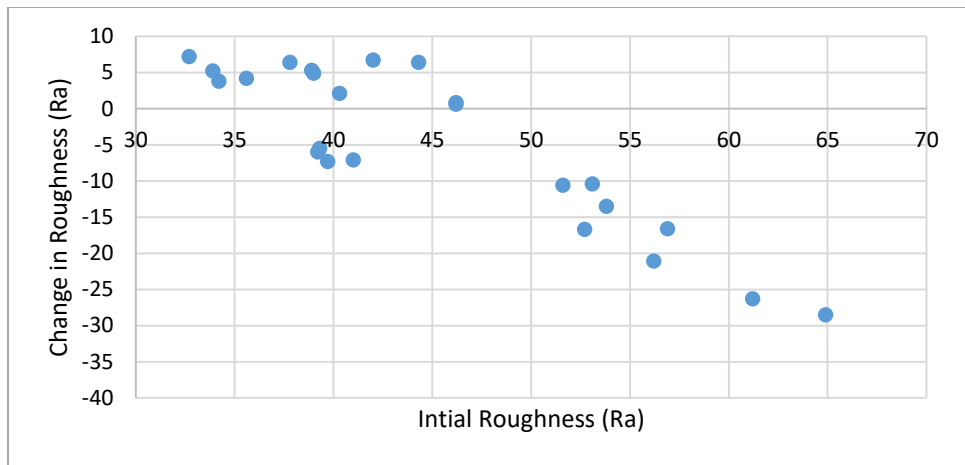
Figure 3.12 Interaction of Initial Surface Roughness and the Post-Burnishing Change in
Roughness (EG5-3.0")

This creates a critical point where burnishing can either increase or decrease the

surface roughness of the component by replacing the as-machined surface roughness.

Secondly, the initial surface roughness was found to not affect the final surface condition with respect to the pre-burnishing state determining the post. However, the relationship between the initial surface condition and the burnishing tool's critical point does influence the post-burnish condition: if a machined surface is significantly rougher, the surface improvement will be more noticeable than if the machined surface has a lower initial roughness.
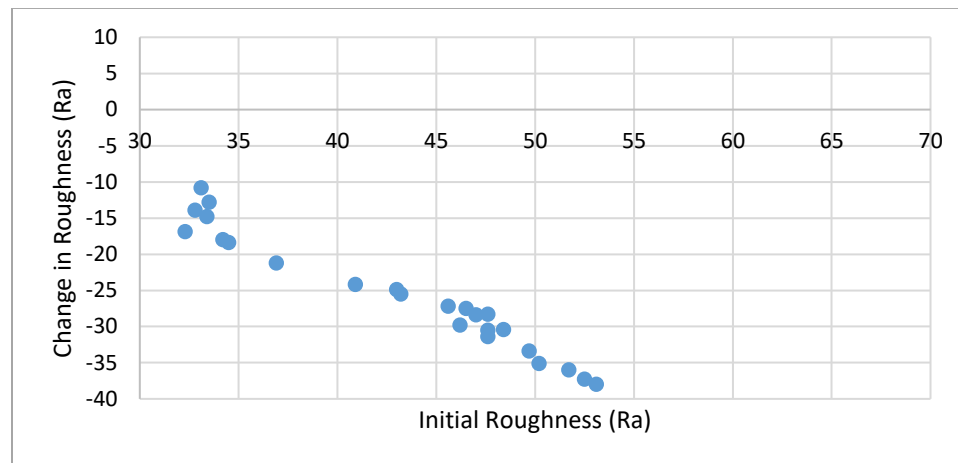
Figure 3.13 Interaction of Initial Surface Roughness and the Post-Burnishing Change in Roughness (HG25)

To support that these conclusions are tool (and parameter) dependent, the same graphical analysis was conducted on the HG25 hydrostatic tool and is shown in Figure 3.13. The HG25 has a larger contact patch than both EG5 rollers and the HG13 unit and exhibited the lowest overall roughness, almost 25 μin lower than the EG5-40M rollers. The same linear relationship between initial and the change in roughness is visible in Figure 3.13 but no horizontal plateau would indicate a critical point was reached within the confines of this experiment. As the average roughness of the post-burnished surface

was ~20 μin and the lowest machined roughness was ~ 30 μin this critical point would not be observed.

It should be stated that this conclusion only applies to feed rates of 0.02"/rev as this was a control variable of DOE 1. A slower feed rate should change the critical point of each tools response. The conclusion that initial roughness does not affect final roughness but instead creates a critical point interaction as a function of tool disagrees with Benghi [2] which stated that "that average roughness is primarily related to the surface finish before deep rolling and less affected by the rolling parameters force and feed". A review of the literature's parameters found that the tools, forces, and feed rates were lower in all categories when compared to this works values. Further comparison between Benghi's process and parameters and the process and parameters used in the current work highlights several key differences in tool geometry, feed rate, and force. The tool used in [2] was a conical tool moved laterally with no specimen rotation using a distance (0.007") between paths as the control and forces predominantly between 11-101 lbf with only a single test using 202 lbs. This is a significantly different region of parameters with rotational feed rates of 0.01-0.03 inches per revolution, high SFM, and larger tool geometries. Additionally, the samples in [2] had a finer machined surface with states roughness values of 27 μin whereas the average roughness in this experiment was almost double this value.

Using the assumption that initial surface roughness does not affect the final roughness values within the confines of this experiment, the two separate DOE results were combined into a single general linear model and examined for statistical difference

and for trends in the main effects. The main effects plot for all six variables with respect to surface roughness is shown in Figure 3.14.
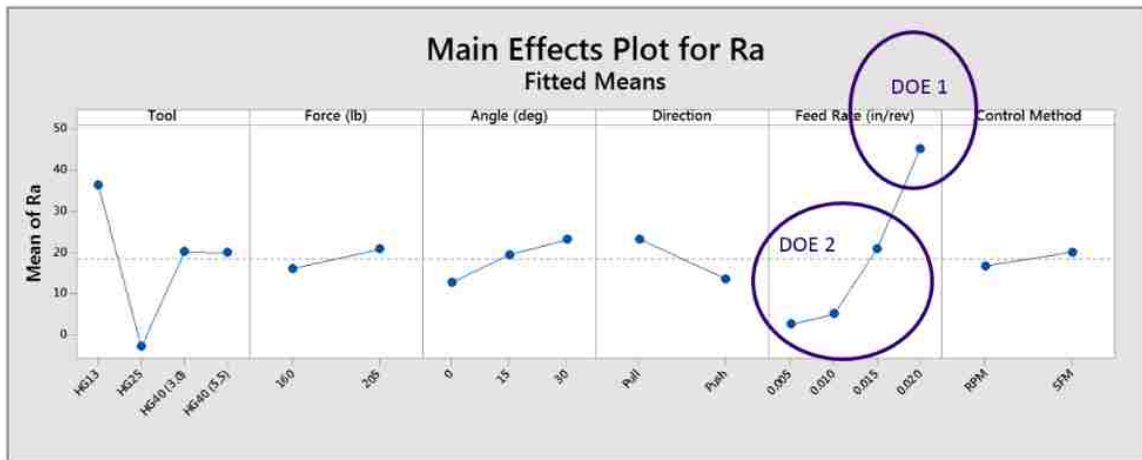
Figure 3.14 ANOVA for Global Experimental Parameters Regarding Surface Roughness

The burnishing tool used for each experimental sub-group contributed such a large component of the standard error (Figure 3.15) that statistical conclusions could not be determined when the all six experimental parameters were analyzed. When the burnishing tool was removed from the analysis, feed rate was the primary driver of surface roughness. Additionally, as noted in Figure 3.14, the feed rates of the two DOE sub-groups were different. The original experimental plan was to use feed rates of 0.01"/rev, 0.02"/rev (DOE 1), and 0.03"/rev to focus on the degradation of residual stress resulting from the lack of plastic deformation overlap. This was changed mid-project due to industrial data and DOE 2 was run with feed rates of 0.005, 0.01, and 0.015"/rev. This did expand the experimental range and revealed the non-linear degradation of surface roughness as a function of feed rate.

Analysis of Variance

Source	DF	Adj SS	Adj MS	F-Value	P-Value
Tool	3	18726.6	6242.20	720.97	0.000
Force (lb)	1	541.7	541.74	62.57	0.000
Angle (deg)	2	1791.1	895.56	103.44	0.000
Direction	1	2210.9	2210.88	255.35	0.000
Feed Rate (in/rev)	3	14095.7	4698.55	542.68	0.000
Control Method	1	265.0	265.00	30.61	0.000
Force (lb)*Angle (deg)	2	77.4	38.72	4.47	0.013
Error	178	1541.1	8.66		
Lack-of-Fit	34	1062.1	31.24	9.39	0.000
Pure Error	144	479.0	3.33		
Total	191	50128.5			

Model Summary

S	R-sq	R-sq(adj)	R-sq(pred)
2.94247	96.93%	96.70%	96.37%

Figure 3.15 Global ANOVA Results

Based on the magnitude of burnishing tool's effect on surface roughness, the response of each tool was separated and analyzed independently to ensure the effects of force and angle were truly significant and not confounded by the difference of each tool. Using the same graphical function of force and angular grouping, Figure 3.16 highlights the difference in roughness response by tool at a constant feed rate of 0.02"/rev and constant RPM of 1,000. The HG13 exhibited the highest roughness while the HG25 exhibited the lowest roughness both due to the interaction between contact diameter and feed rates. The EG5-40M 3.0" and 5.5" rollers exhibited identical surface roughness responses which supports that minor diameter (0.1875" radius) is the primary driver of contact stress, not the major diameters, which aligns with Hertzian contact stress analysis.

From a main effect's perspective, when tool and feed rate are separated from the statistical model, the effect of burnishing force and angle are similar and linear for all three tools as shown in Figure 3.17 a, b, and c. Results for the EG5 – 3.0 were removed

from this comparison due to the mixed feed rates resulting from the statistical design. This supports that surface roughness responses are similar regardless of the burnishing tool utilized. This validates a critical assumption of this work and justifies global trend analysis resulting from data generated from a specific tool.
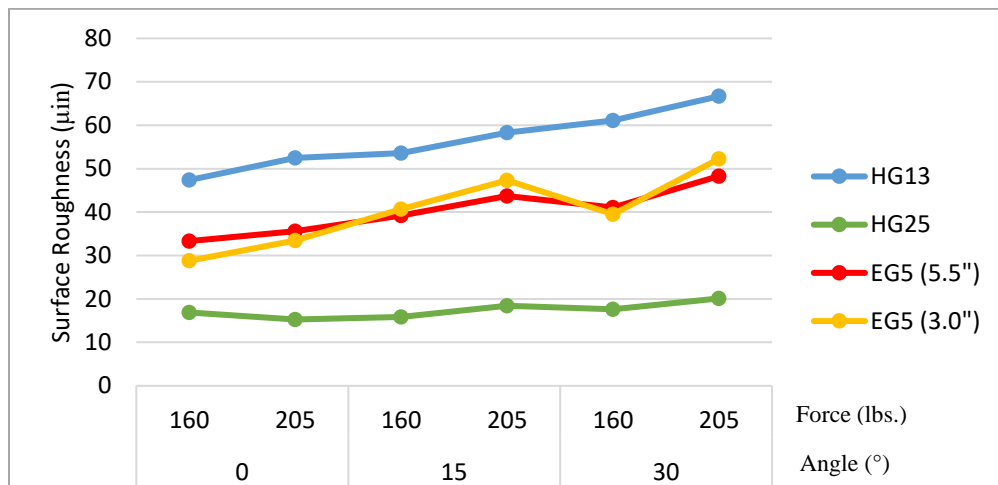
Figure 3.16 Surface Roughness as a Function of Tool

The EG5-3.0 tool was unique as it was the only tool used in DOE 2 which focused on feed rates and surface velocity control methods. This burnishing tool connects the two statistical designs following the validated assumption that trends are similar between tools. The non-linear trend in surface roughness resulting from feed rate (Figure 3.18) is apparent and the trend is assumed universal with the offset being tool specific. Two separate conclusions drawn from the analysis of the EG5-3.0" is that spindle RPM is not a significant variable between values of 500 and 1,000 but that there is a difference in roughness following SFM control.
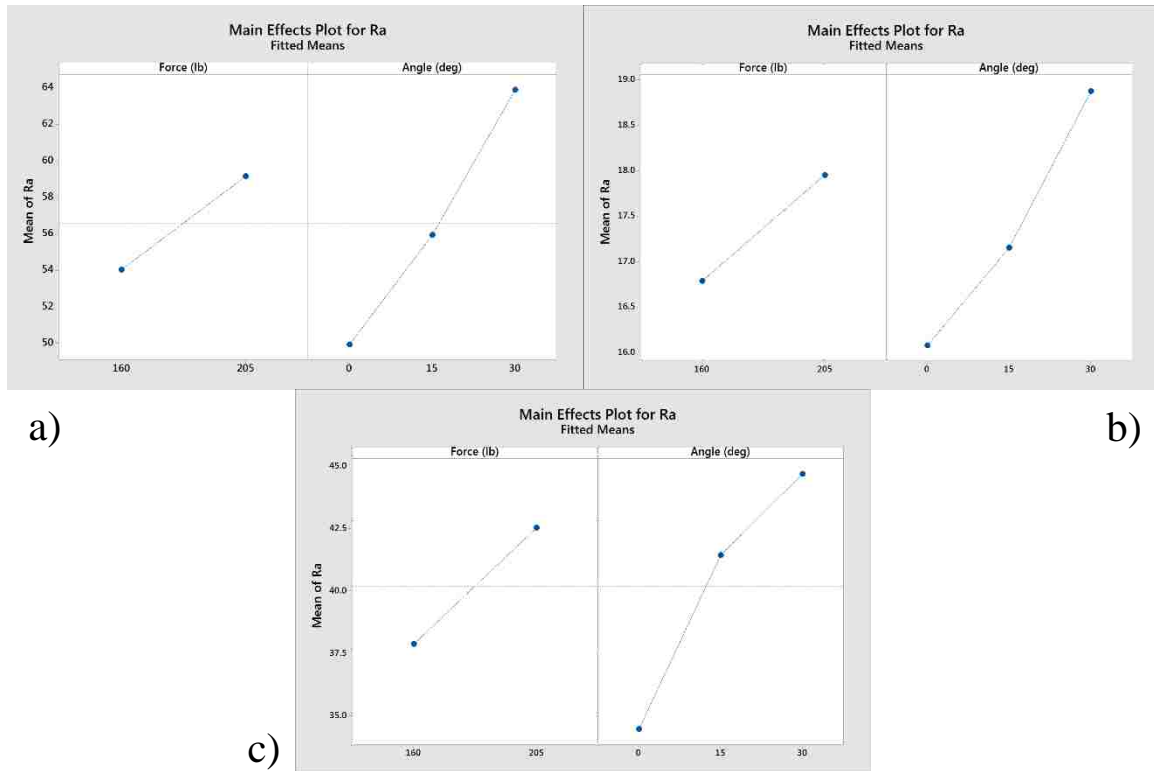
Figure 3.17 ANOVA Main Effects of Force and Angle Separated from Tool a) HG13 b) HG25 c) EG5-5.5

However, when the control method (RPM vs. SFM) was separated from the parameter's magnitude (500 vs. 1,000) the main effects of the magnitude could not be determined due to statistical insignificance. Therefore, the control method for the specimen sizes used was found to not impact the surface roughness. When processing industrial sized products, this relationship could change as a constant RPM will result is significantly larger surface velocities and SFM control will result in lower RPM's.

With respect to direction of movement, the relationship between tool angle and feed rate (Pushing vs. Pulling) is an industrial concern due to the increase in robotic tool holding in burnishing processes. This increase in motion and position control allows for

more design freedom regarding all processing parameters and can be used to further improve the process's benefit.
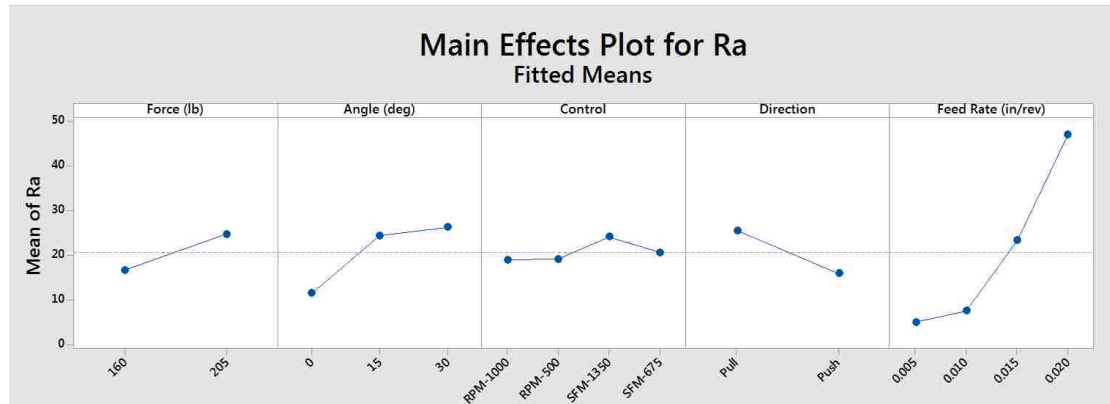
Figure 3.18 ANOVA Main Effects Using the EG5-3.0 Tool

When the data was normalized to separate the trends in the direction, a stark difference was found regarding surface roughness. When roughness was graphed as a function of both feed rate and angle regardless of force or control method, the response was separated by the directionality as graphically shown in Figure 3.19.

General conclusions can be drawn from the work characterizing the effects of the deep rolling process parameters on surface roughness. First, the burnishing tool is the primary contributor towards surface roughness with larger radii generating the lowest roughness values. With respect to the other parameters, they are listed in order of significance: feed rate, tool angle, tool direction, burnishing force, and for small specimens, the control method utilized.
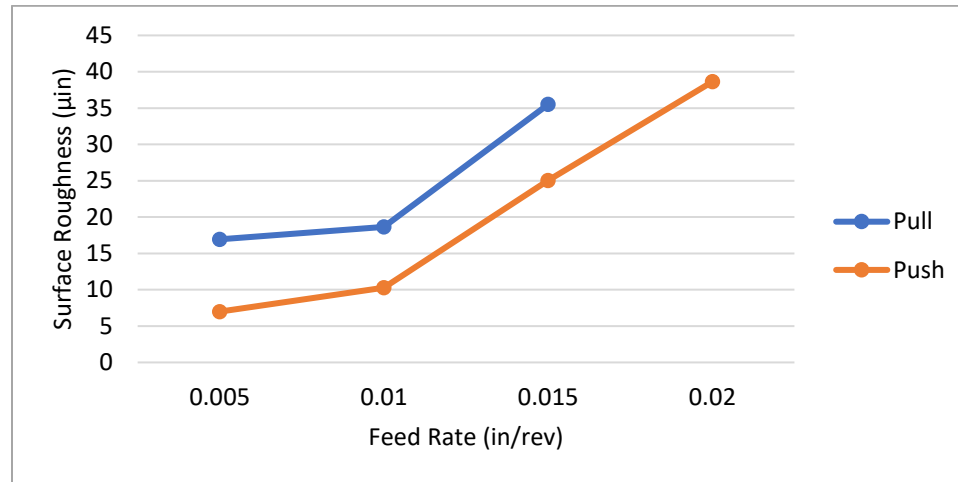
Figure 3.19 Surface Roughness Comparison as a Function of Feed Rate and Relative Directionality

3.4. RESIDUAL STRESS

Based on the tables shown in Appendix A and B, there were a total of 51 samples manufactured for this work: 8 groups within the DOE's containing 6 samples each with an additional sub-group of 3 to provide resolution regarding the effects of lower forces (115 lbs.). Due to errors in the procedure and analysis, a total of five data samples were invalidated, decreasing the resolution of the experiment but maintaining sufficient statistical resolution as at most, one of each sub-group was eliminated. The initial sample analyzed was in the as-machined state. When discussing the effect of machining on residual stress states, Stephens [15] found that surface condition is heavily dependent upon the production parameters, but that most commonly a tensile residual stress is produced from chip formative machining processes. Therefore, it was deemed prudent to quantify the extent of this tensile stress states as it could affect the post-burnish condition. The HD result for the baseline sample showing a stress state between -2 ksi and 0.5 ksi is provided in Figure 3.20. Compared to the -20 ksi to -40 ksi measurements seen in the

remainder of the study, this 2.5-5.0% offset was deemed negligible within the 10-30%

error band that is standard for the HD method [13].
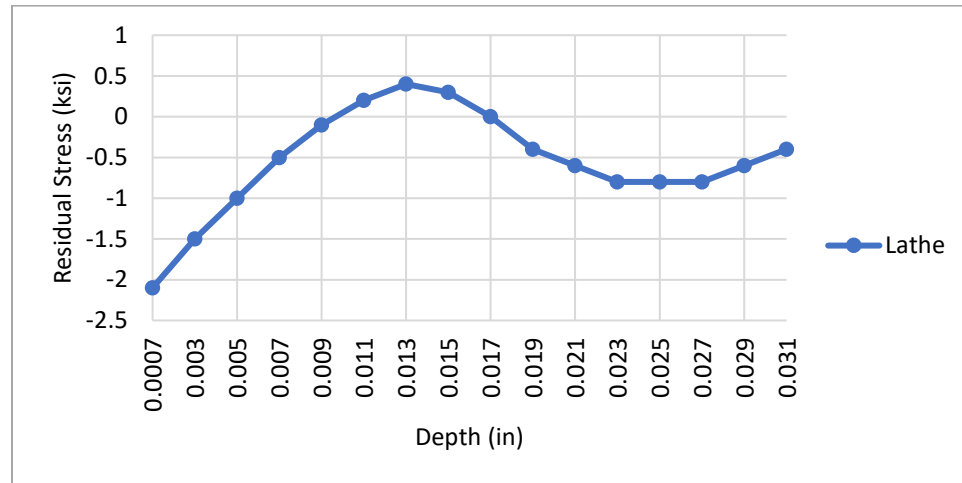
Figure 3.20 As-Machined Residual Stress State

Although previously reviewed, a greater investigation into the response variables

of this work should be discussed. Abrão, et al. [1] discusses the gradient of residual

stress (in steel) as forming due to Hertzian stresses that resolve at their maximum below

the materials surface. This relates well to both empirical results shown in Figure 3.21

and FEA results derived from a previous industrial project using ANSYS 17.1 and elasto-

plastic AA6061 material properties and a rigid spherical roller shown in Figure 3.22.

This non-uniform residual stress profile presents a complexity to characterization

in that 2D curvatures do not present obvious variables for comparing except for RMS

error terms which compare an experimental curve to a baseline value. This in and of

itself only states how dissimilar a curve is and would do little to further a parameter

optimization.
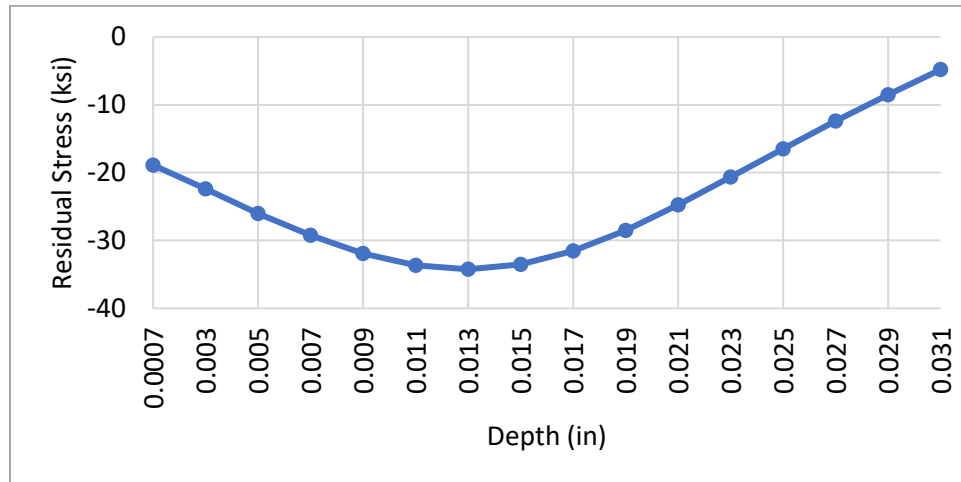
Figure 3.21 Residual Stress vs. Depth Curve Highlighting the Maximum Compressive
Stress Occurring at 0.017" Depth
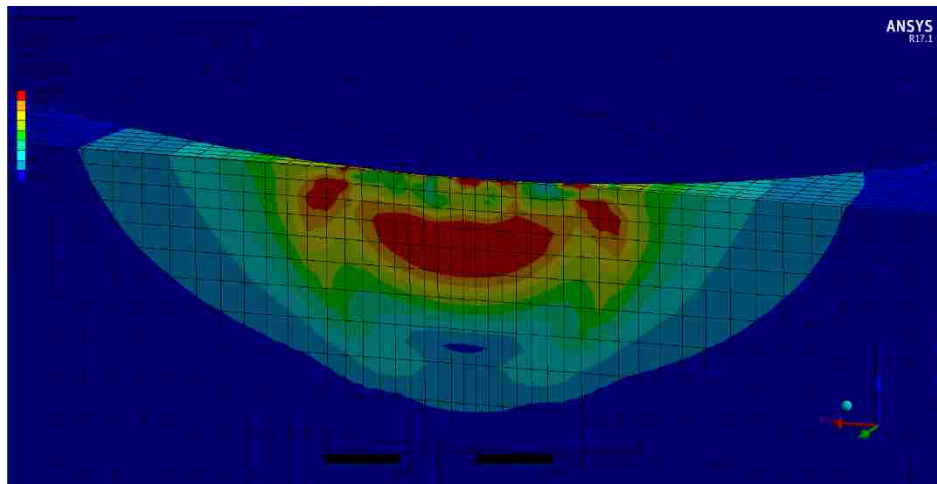
Figure 3.22 Hertzian Contact Stress Maximum Occurring Sub-Surface (ANSYS 17.1)

Therefore, the residual stress profile was broken down into five unique
components: Depth of Maximum Compressive Stress, Maximum Compressive Residual
Stress, Compressive Stress at Surface, Compressive Stress at 0.031" Depth, and the
Principle Angle at Surface. The initial analysis utilized a global general linear model
ANOVA, which were processed with Minitab 17. Each of the five responses were

analyzed separately, generating 5 distinct ANOVA tables using the factors and levels as

shown in Figure 3.23

```
Factor             Type   Levels  Values
Tool               Fixed      4   EG5 (3.0), EG5 (5.5), HG13, HG25
Force (lb)         Fixed      3   115, 160, 205
Angle (deg)        Fixed      3   0, 15, 30
Direction          Fixed      2   Pull, Push
Feed Rate (in/rev) Fixed      4   0.005, 0.010, 0.015, 0.020
Method             Fixed      2   RPM, SFM
```

Figure 3.23 Global Residual Stress ANOVA Levels and Factors

It should be noted that "Control" was split into two separate variables: Methods

and RPM. The Method states whether the G-code used to produce the sample controlled

RPM or SFM. However, it was found treating Method as a categorical variable (RPM-

1000 or SFM-1350) overlooked the surface dynamics (the instantaneous velocity). As

stated in the methodology, all measurements (roughness and residual stress) were taken

2.4" from the specimen center, therefore controlling SFM would result in a specific RPM

(or vice versa) at that point. A SFM value of 675 generated an RPM of 537 and a SFM

value of 1,350 generated an RPM of 1,074. Therefore, these two separate control

methods result in almost identical surface dynamics at a radius of 2.4" when compared to

RPM control (500/1,000); these results would be significantly different on a larger

specimen. The ANOVA results of the global analysis found no significant difference due

to RPM and excluded it from the results.

The ANOVA main effects plots are shown in the Appendix C, but the overall

conclusion was inconclusive as there was no consistency between the five response

variables and the predictors. Using $\alpha=0.05$, the p-values from each ANOVA are shown

below in Table 3.6. Based on the percentage significant, it is obvious that the
experimental variable burnishing tool is always significant in affecting all five response
variables with respect to residual stress. The second most significant parameter was the
direction (push vs. pull) which is interesting giving that Mahajan et al's [6] literature
found that direction was only discussed in 7% of the reviewed literature.

Using the results from the surface roughness ANOVA as a guide, the
experimental variable burnishing tool could confound the results of the other variables.
To investigate this, the Adjusted Sum Squares values were extracted from the ANOVA
tables and converted into a percentage of total variation (Table 3.7).

Table 3.6 ANOVA P-Values of Global Residual Stress

p = 0.05						
	Tool	Force (lb.)	Angle (deg)	Direction	Feed Rate (in/rev)	Method
Depth of Max. Comp. Stress	0.00	0.00	0.01	0.01	0.28	0.16
Max. Comp. Stress	0.00	0.88	0.02	0.02	0.01	0.80
Comp. Stress at Surface	0.00	0.94	0.09	0.00	0.16	0.62
Comp. Stress at 0.31" Depth	0.00	0.00	0.43	0.98	0.01	0.07
Principle Angle at Surface	0.00	0.45	0.70	0.00	0.43	0.98
% Significant	100%	40%	40%	80%	40%	0%

These results suggest that burnishing tool is the primary driver for experimental
variation and possibly confounded the statistical conclusions as 40% - 68% of the
variation resulted from this single variable. When the tool was removed from the global
analysis and a separate ANOVA was completed per tool, it was found that Force and

Angle were not statistically significant until additional variables were added under the

EG5-40M 3.0" roller.

Table 3.7 Percentage of Total Error using Adjusted Sum Square ANOVA Results

	Tool	Force (lb.)	Angle (°)	Direction	Feed Rate (in/rev)	Method
Depth of Max. Comp. Stress	46.4%	18.0%	14.3%	12.8%	5.6%	2.9%
Max. Comp. Stress	47.3%	0.5%	16.8%	11.5%	23.7%	0.1%
Comp. Stress at Surface	40.8%	0.2%	8.0%	42.2%	8.3%	0.4%
Comp. Stress at 0.31" Depth	61.0%	24.6%	1.4%	0.0%	10.2%	2.9%
Principle Angle at Surface	68.4%	3.2%	1.4%	21.5%	5.5%	0.0%

This statistical insignificance could be a result of low repetition population and

low magnitude differences resulting from the experimental variables. Majzoobie [7]

found that in 7075-T6 aluminum, it was possible to over-process the surface due to the

formation of micro-cracks. Although micro-cracks were not searched for within this

work, over plasticity could result in diminishing gains with respect to residual stresses.

As the ANOVA results for the five separate response variables did not yield conclusive

results due to analysis limitations, a single factor analysis approach will be considered to

document the effect of each primary parameter.

3.4.1. Burnishing Tool. The focus of DOE 1 was the interaction between tool,

burnishing force, and tool angle while maintaining a 0.02"/rev feed rate at a constant

1,000 RPM and pushing the material. The assumption within Figure 3.24 is that the

effect of force and angle have a comparable offset, therefore an average line comparing tools is accurate.

The graphical analysis in Figure 3.24 supports the conclusions of the ANOVA analysis in that the burnishing tool selected does have a significant effect on the residual stress state. Additionally, a clear trend differentiating between hydrostatic and roller burnisher exists where the hydrostatic tools (regardless of contact patch area) produced a more compressive and deeper residual stress profile than the roller burnishers. No reviewed literature analyzed the difference between tools in a single study, most studies [5, 8, 10, 20] utilized a hydrostatic tool with [7] using a roller burnisher (not including shot peening).
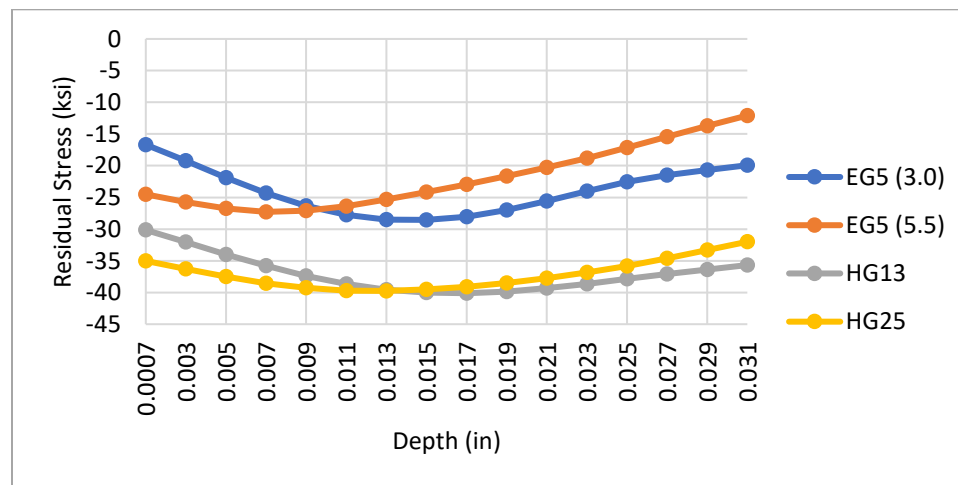
Figure 3.24 DOE 1 Residual Stress Comparison as a Function of Burnishing Tool

Wong et al [20] did utilize three separate tools, however each tool was custom to a specific interface geometry and did not involve a discussion of the 2D residual stress profile based on tool contact regions or dynamics. Based on an objective to maximize the

compressive residual stress, hydrostatic elements clearly show supremacy over bearing based burnishers. However, it should be noted that cycle time is normally more limited with hydrostatic tools than roller burnishers. The relative depth of residual stress was not found to matter significantly between each tool as the maximum compressive stress normally occurred between 0.015" and 0.017" below the materials surface.

3.4.2. Burnishing Force. Burnishing force is the simplest and least expensive parameter to modify within the production environment, often being modified through tool offsets or air/hydraulic pressures. This parameter has also proven to be an effective parameter to increase fatigue performance in lighter weight components as a 25% increase in burnishing pressure added enough compressive residual stress to offset a 30% increase in maximum principle stress due to field loading. As the average residual stress profiles were similar for the two classification of roller tools, Figures 3.25 and 3.26 present the average residual stress vs. depth curves for each classification of tool: hydrostatic or roller burnisher. In the global sense, increasing the force from 160 lbs. to 205 lbs. increased the residual stress by 2-5 ksi.

The hydrostatic tools resulted in similar shape and magnitude of profile with the increase in force resulting in a 3 ksi offset and a slightly deeper residual stress. When each tool was compared at identical forces, no significant differences were observed which contradicted an original assumption relating to contact patch influencing the residual stress profile.
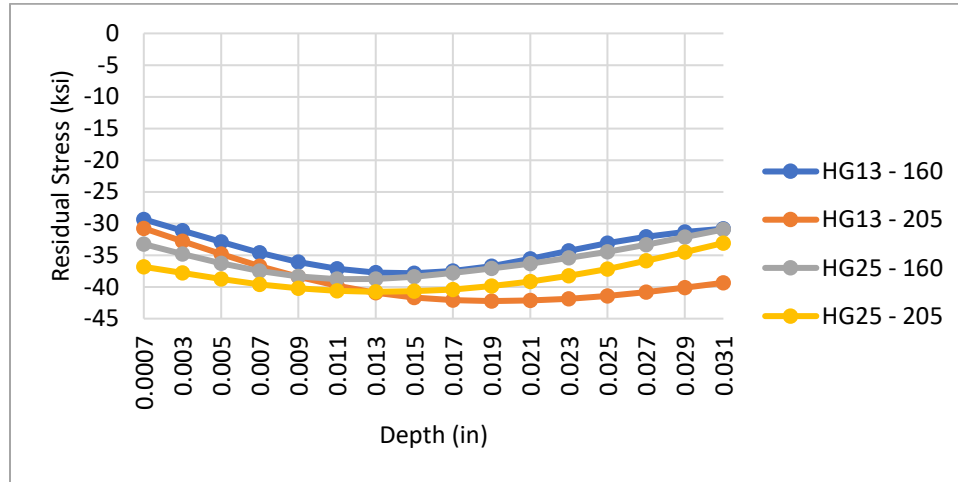
Figure 3.25 Residual Stress as a Function of Hydrostatic Tool and Force (lbs.)
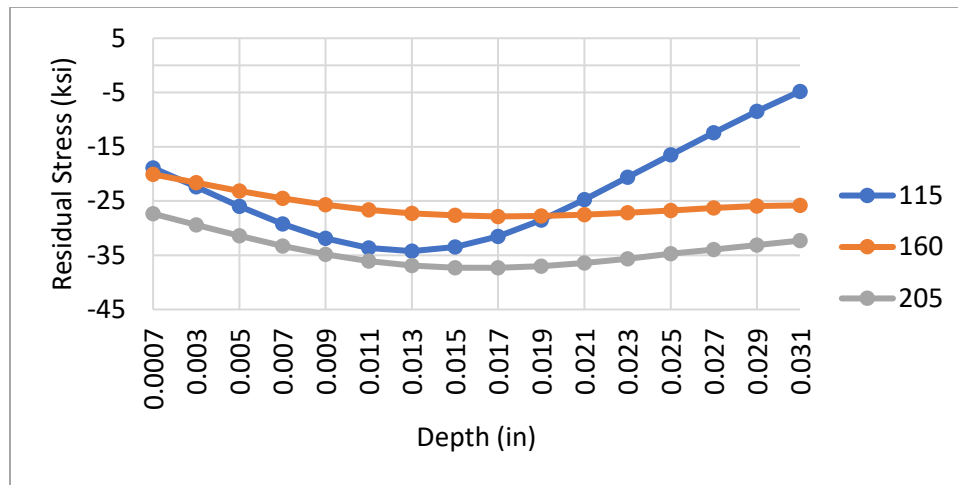
Figure 3.26 Residual Stress as a Function of Burnishing Force (lbs.) – EG5

When using three-dimensional calculation of contact patch utilizing Hertzian contact patterns, the HG13 had a calculated contact area of 0.57 mm^2 while the HG25 had an area of 0.87 mm^2. With identical burnishing forces, the contact pressure was assumed to be a driving element (function of force and roller diameters). These results

challenge this assumption in Aluminum as the sub-surface residual stress profiles were nearly identical.

When inspecting the results from the roller burnisher (Figure 3.26), some form of discrepancy was found relating either to the 115 lb. or 160 lb. data group as the more compressive trend following burnishing force was not followed. It should be noted that the EG5-3.0 tool was the only sample group to contain the 115 lb. force which provided valuable information concerning depth and force relationship. In all four tools, the burnishing forces of 160 and 205 lbs. did not result in a visible zero or tensile residual stress profile as the material attempts to reach an equilibrium within the depth of analysis (0.031"). The 115 lb. group however does show a clear trend towards the neutral axis, therefore the range between 115 and 160 lbs. results in a clear response change between the depth and burnishing force.

3.4.3. Tool Angle Relative to Surface. Historically tool angle was not a design variable, it was a limitation constrained between production and tooling recommendations. The EG5-40M tools and the hydrostatic tools specify a maximum angular deviation of 30º from surface normality. Past practice in industry was to design a static fixture within a machine, such that a region of the product could be burnished with the least number of burnishing tools. A common automotive component could require up to five separate tools to adequately reach all surfaces using this practice. With industry increasing its utilization of robotic burnishing cells, the tool's angularity with respect to the surface normal is now a truly variable design parameter that can be specified. The residual stress plots as a function of angle separated by the four burnishing tools are shown in Figure 3.27.

The results show a weak relationship between increasing angle and an increase in residual stress. Additionally, the EG5 rollers show an increase in residual stress variation as angle increases. This could be a result of the plastic wake that forms in front of the burnishing direction as discussed by Beghini [2]. As the tool angle is increased, more lateral force is placed on the surface of the component which would increase the plastic zone wake in front of the tool due to material plastic deformation. This would increase the deformation energy being placed into the surface and could increase the residual stress. If the tool is perfectly normal to the surface (0°) than the height of the plastic zone height is only a function of the displaced material.
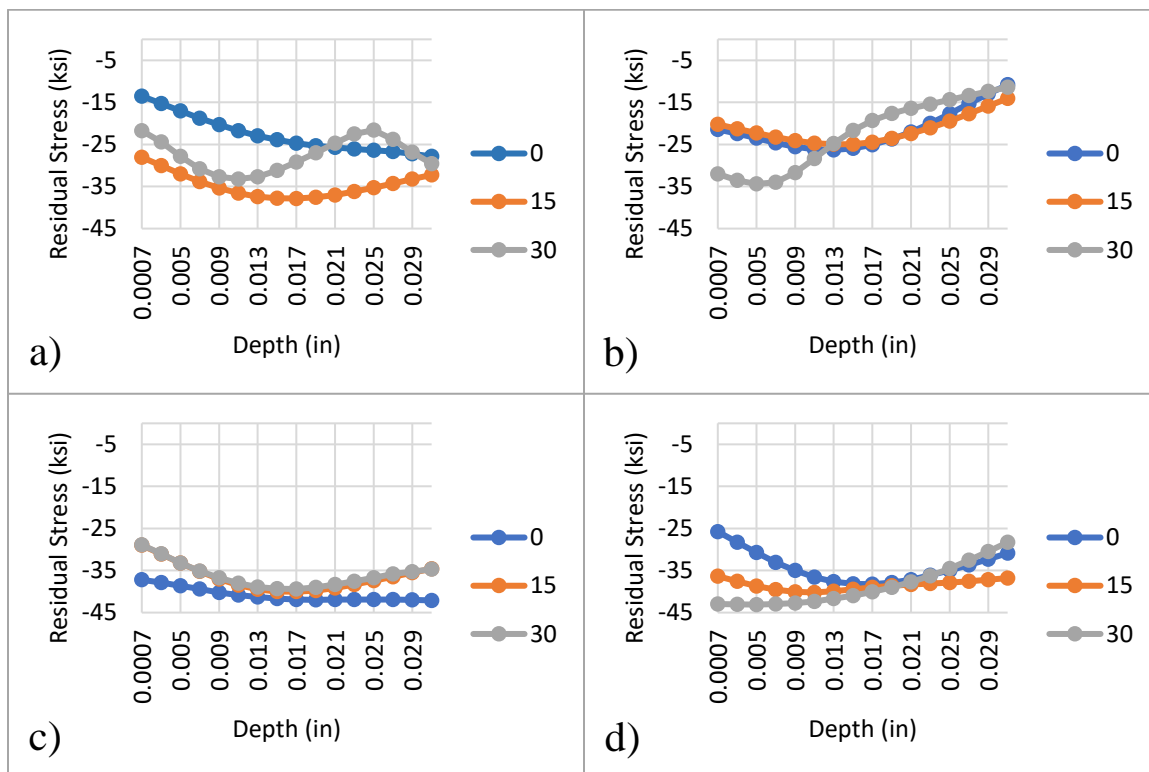
Figure 3.27 Tool Angle's Effect on Residual Stress vs. Depth Profile (°) a) EG5-3.0"
b) EG5-5.5" c) HG13 d) HG25

3.4.4. Feed Rate.   Wong, et al. [20] found little correlation between the feed rate

of a hydrostatic burnishing tool and the resultant residual stress within titanium. The

results shown in Figure 3.27 do not support this conclusion. Wong, et al. [20] utilized a

single pass tool on a single linear path whereas the samples of this work were rotationally

burnished. The results for the residual stress profile as a function of feed rate is shown in

Figure 3.28 and reveal a non-linear decrease in residual stress as feed rate increases. It

should be noted that the feed rate's non-linear decrease in residual stress inversely

mirrors the increase in roughness as a function of increasing feed rate. This could

support some form of relationship between roughness and residual stress for a single tool.

The data presented below was produced using the EG5-3.0 tool.
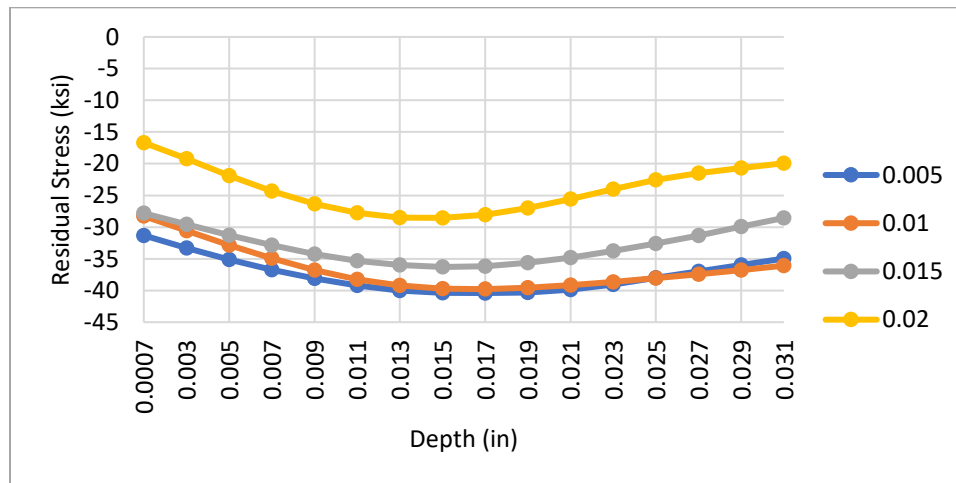
Figure 3.28 Feed Rate's (in/rev) Effect on Residual Stress Profile (EG5-3.0")

3.4.5. Direction of Burnishing.   The direction of burnishing is dependent upon

the tool's angularity. If the tool is normal to the surface, this parameter is equivalent

between the two groups. To ensure physical differences were observed while

investigating the relative direction of movement, all samples in DOE 2 were produced

with the burnishing tool at 15º from surface normal. The effect of directionality on the

residual stress curve is provided in Figure 3.29. Separating feed rate (in/rev) into groups

highlights the consistency between variable groups. The directionality appears to affect

the formation of residual stress.
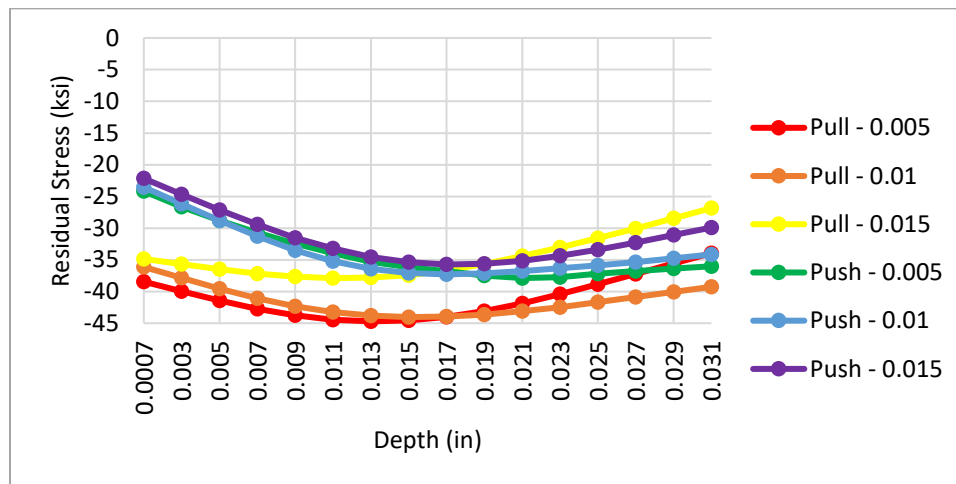
Figure 3.29 Directionality's Effect on Residual Stress Including Feed Rate (in/rev) -
EG5- 3.0"

A limitation of this conclusion should be discussed concerning the functionality

of the tool utilized. Although previously mentioned, the Ecoroll EG5 burnishing tools

utilize a spring pack to generate the burnishing force which is displacement dependent.

Contrast this to hydrostatic tooling which generate consistent force throughout its stroke

as a function of fluid pressure. To calibrate the force on each sample, the tooling was

pressed into the sample at either the extreme outer or inner radial location to ensure the

proper lathe offset and therefore the correct force. Any changes in surface condition

could result in more or less force being generated, specifically focusing on the possibility

of an interaction between the plastic zone wake discussed by Beghini [2] and highlighted

through FEA simulation (Figure 3.30). An additional mechanical cause for the difference

in residual stress profile is tool rigidity. The EG5 tool design is not symmetric with a

single side exhibiting most of the rigidity. In discussion with Ecoroll, it was stated that

the tool has a preferred orientation to ensure consistent tool deflection and internal

friction which could affect applied force and the resulting surface condition.
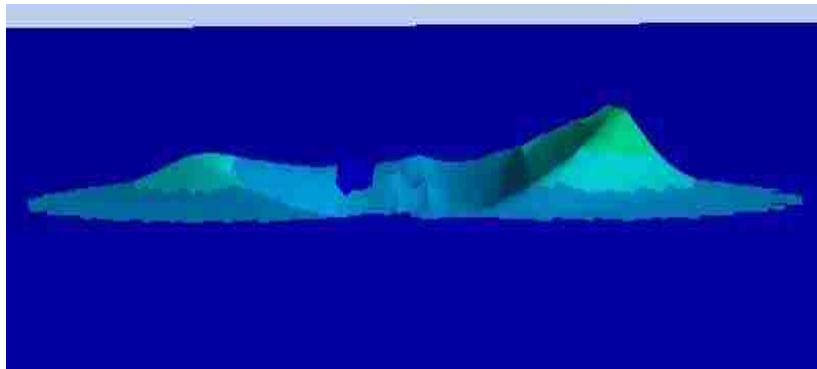
Figure 3.30 Plastic Zone Wake due to Roller Burnishing (ANSYS)

3.4.6. Control Method. Two control methods were used in this project each

with two parameters. Ecoroll recommends SFM control when using all hydrostatic tools.

Additionally, industry guidelines recommend 675 SFM max but allow up to 1,350 SFM

with increased risk to surface finish and tool life degradation. Industry experience with

roller burnishing has seen more utilization of RPM control between the ranges of 500 and

1,000 RPM's. Figure 3.31 supports that there is no correlation between control method

and the formation of residual stress. As discussed earlier, the SFM parameter was

converted into instantaneous RPM at 2.4" radial location which revealed SFM 675 ≈

RPM 500 and SFM 1,350 ≈ RPM 1,000 which was an unfortunate oversight during the experimental design.
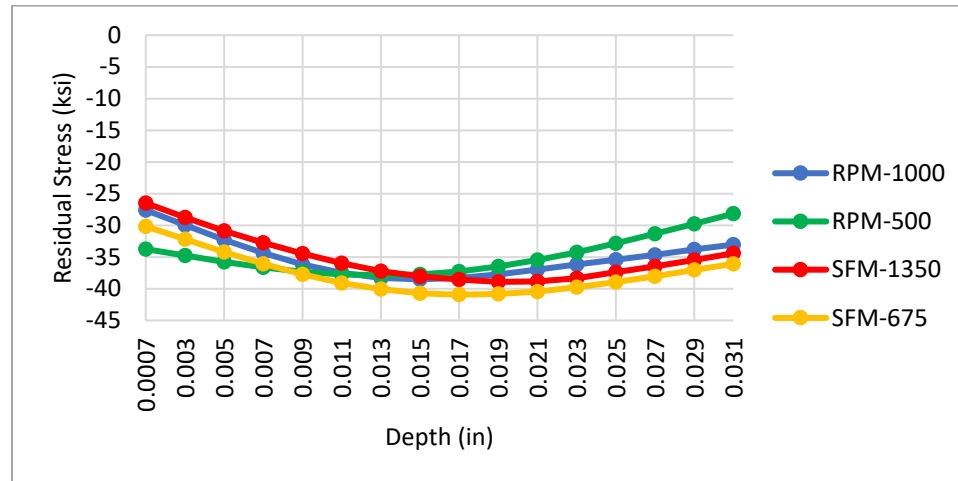
Figure 3.31 Control Method's Effect on Residual Stress (EG5-3.0")

3.5. CORRELATION BETWEEN ROUGHNESS AND RESIDUAL STRESS

A major concern within modern industrial facilities that utilize burnishing to improve the fatigue resistance of components is reliable and feasible methods to determine the presence of compressive residual stresses. As discussed in this work, two predominant methods exist to measure residual stresses: Hole Drill and XRD methods. The issues with these procedures are cost, time, or operator expertise. Roughness is a common quality metric in industry because speed, simplicity, and affordability of measurement. As shown previously, Ra is a reliable metric to differentiate between different burnishing parameters. If the surface is sufficiently above a specific tool's critical point at a certain feed rate, a significant surface change will be measurable and visibly different if burnishing has occurred. Although it was stated that the four residual

stress parameters were insufficient to determine statistical significance between resulting

stresses as a function of industry parameters, these residual stress parameters were also

analyzed for correlation with surface roughness. Pearson correlation values and a P-

value with a 95% confidence interval were utilized to determine if a significant

correlation exists. The results of this analysis are summarized in Table 3.8.

Table 3.8 Correlation Parameters of Roughness and Residual Stress Values

$\alpha=0.05$		
	Pearson Correlation Value	p-value
Depth of Max. Comp. Stress	0.063	0.756
Max. Comp. Stress	0.438	0.022
Comp. Stress at Surface	0.196	0.327
Comp. Stress at 0.31" Depth	0.553	0.003
Principle Angle at Surface	0.121	0.548
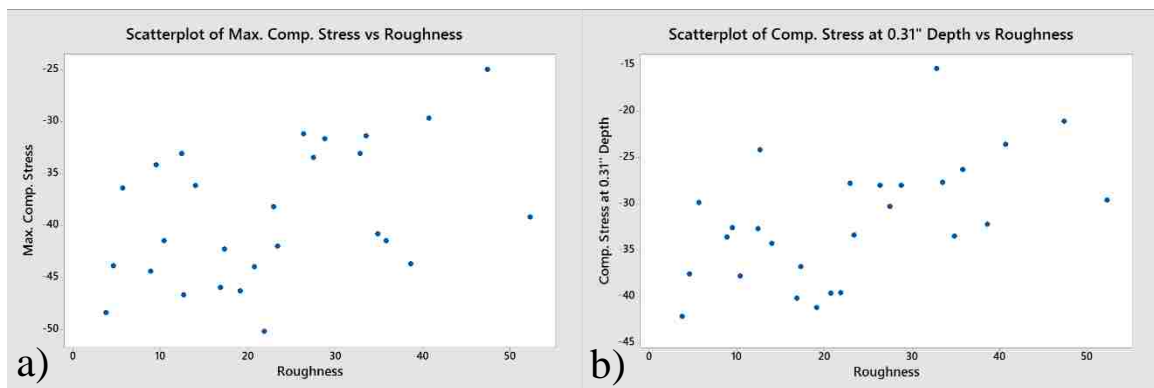
Figure 3.32 Correlation between Surface Roughness (Ra µin) and a) Maximum
Compressive Stress and b) Compressive Stress at 0.31" Depth (EG5-3.0")

The results of the single parameter support a weak correlation between surface roughness and Maximum Compressive Stress and the Compressive Stress at 0.31" Depth. Figure 3.32 contain the two scatter plots showing the correlation values. This correlation is logical when recalling the non-linear increase in roughness as feed rate increased and the non-linear decrease in residual stress as a function of feed rate.

This correlation is only valid when comparing results from a single tool as the statistical significance of the burnishing tool selected overrides all other experimental parameters. If the two tools are similar (EG5-3.0 vs. EG5-5.5 or HG13 vs. HG25), this work would suggest that trending between similar tool mechanisms could be valid, but more work would be required. Increasing the surface roughness of the initial component, when combined with a knowledge of the roughness change as a function of burnishing parameters should allow industrial quality departments to approximate the presence of residual stress. However, this does not replace the need for frequent measurements of the residual stress profile through direct methods, especially for safety critical components.

3.6. PRINCIPLE STRESS ORIENTATION

Residual stress is assumed to be in a planar stress state [12, 13, 14] which is an assumption that greatly simplifies and allows the integral method for calculation of residual stress. From the perspective of bending fatigue, surface stresses are also often simplified to a 2D stress state, which would allow superposition of the two stress states to determine interactions between applied load and internal residual stresses. However, when a geometric discontinuity is added into the sample, the stress state becomes more complex with the inclusion of stress risers, geometric discontinuities, and multi-variate

loading. Beghini, et al [2] states that the principle compressive stress directions were aligned in the direction of the rolling velocity which was used as the baseline assumption when aligning the HD strain gages (radially away from center as the X-axis). Therefore, if the principle stress direction was 90° this would support literature conclusions regarding the alignment of residual stress, but also offer the opportunity to determine if orientation was affected by other parameters. With this information, designers may be able to modify the orientation of residual stresses to better mitigate the damage by fatigue. Angle of principle stress was analyzed using ANOVA and two separate parameters were found to be statistically significant: burnishing tool and directionality. Figures 3.33 and 3.34 both depict the principle direction of the residual stress as a function of depth, however the first illustrates the effect of burnishing tool and the second shows the effect of force and relative tool direction.

The effect of burnishing tool was found to be split between burnishing system with hydrostatic and roller burnishers maintaining separate groups. The results support that the general orientation of the maximum principle stress is along the rolling direction, however there was a ±10 ° deviation depending on the tool selected. As the maximum principle stress is the most tensile (largest), the minimum principle stress is the most compressive. Therefore, the orientation of the most compressive stress is perpendicular to rolling direction, or aligned with the feed rates direction. Currently, the geometry of the contact patch (circular vs. oval) is the primary justification for this variation. With respect to the difference resulting from direction of burnishing, the data collected was only for the EG5-3.0" roller burnishing tool. The results included Force to differentiate

the variation found within the results of this tool, which was not observed within the hydrostatic roller.
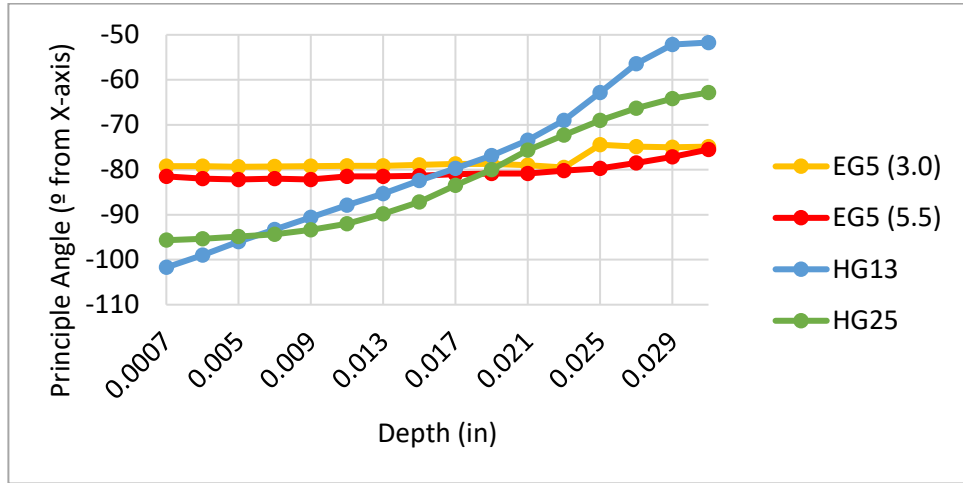

Figure 3.33 Principle Stress Direction vs. Depth – The Effect of Tool
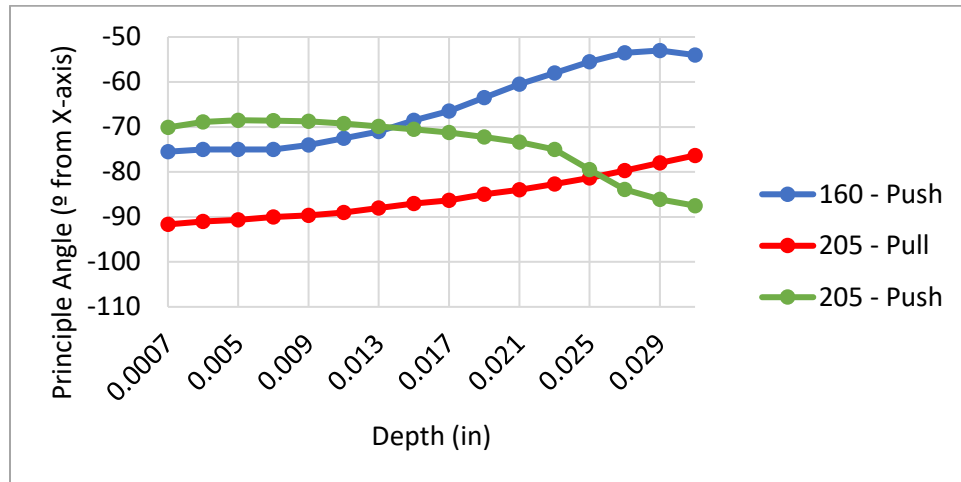
Figure 3.34 Principle Stress Direction vs. Depth – Force (lbs.) and Directionality (EG5-3.0")

4. CONCLUSIONS

This study found that Ra was the most reliable surface roughness measurement parameter to detect changes resulting from the selected industrial parameters. All of the investigated industrial parameters were found to be statistically significant with respect to the final surface roughness. The form of burnishing tool used was the most significant, with the roller burnishing tools producing the same average roughness and the HG25 generating the best finish. The HG13 generated the worst finish due to its smaller contact size and high feed rate. Feed rate was the second most critical parameter, exhibiting a non-linear response as feed rate increased. Force and Angle affected roughness in a similar magnitude, while the directionality of the burnishing process was related to the angular offset of the tool. The control method and magnitudes of each had the least effect on the final roughness.

The formation of residual stress was also found to be most affected by the burnishing tool, with the primary difference being hydrostatic compared with roller burnisher. The hydrostatic tools generated the most compressive residual stress independent of contact area and the two roller burnishing tools generated similar residual stresses. Feed rate was the second most critical parameter with a non-linear degradation of residual stress as a function of feed rate visible in the data. When force was decreased below 160 lbs. but above 115 lbs., the depth of residual stress begins to decrease with a significant loss of depth visible at 115 lbs. The Directionality of burnishing was found to affect the residual stress profile due to interactions between the plastic wake formed at the tool tip and the vector of velocity creating a multi-axial force that was resolved by the

burnishing tool's mechanism. An increase in burnishing tool angle showed a weak

correlation with an increase in residual stress, but also increased the scatter of results for

the roller burnishing tools. Due to the similar trends in roughness and residual stress as a

function of feed rate, surface roughness showed a statistically significant positive

correlation between feed rate and both max compressive residual stress and the residual

stress at 0.031" depth for a specific tool. Initial surface roughness was not found to affect

the final roughness if the as-machined finish was greater than 45 μin Ra for the roller

burnishers. Finally, the principle stress direction was found to be in the primary rolling

direction which results in the minimum principle stress being aligned with the direction

of feed rate. However, differences did exist based on the tool used, with hydrostatic and

roller burnishers forming distinct groups within ±10° of the rolling direction. This

difference is attributed to the difference in contact patch geometry between the two tool

styles and the lack of physical rotational constraints on the hydrostatic tool.

5. FUTURE WORK

The results of this study show that the common industrial parameters affect both roughness and residual stress fields after the burnishing operation in AA6061-T6. However, due to the extent of the differences between the hydrostatic and roller burnishing tools, DOE 2 (Feed rate, direction, and control method) should be repeated using a hydrostatic tool as the only tool used to investigate these parameters was the EG5-3.0. Since the tools within these two groups behaved similarly, it will be assumed comparable to only test a single hydrostatic tool. Additionally, work should be done to confirm the effect of yield strength and strain rate sensitivity/hardenability through the use of modified heat treatment cycles to over and underage the material.

Micro-hardness is also a variable of interest for additional work. Several of the stress values exceeded yield stress values of the material which could support the presence of localized hardening. As yield stress and hardness can be corelated, the presence of a micro-hardness gradient similar to the stress gradients observed in this work would support that some processes could increase not only the magnitude of the compressive residual stresses above the material's bulk yield strength but also work harden the surface to improve fretting fatigue performance.

APPENDIX A

DOE 1 EXPERIMENTAL DESIGN

Tool	Force (lb.)	Angle (deg)	Control	Direction	Feed Rate (in/rev)
HG13	160	0	RPM-1000	Push	0.02
HG13	205	0	RPM-1000	Push	0.02
HG13	160	15	RPM-1000	Push	0.02
HG13	205	15	RPM-1000	Push	0.02
HG13	160	30	RPM-1000	Push	0.02
HG13	205	30	RPM-1000	Push	0.02
HG25	160	0	RPM-1000	Push	0.02
HG25	205	0	RPM-1000	Push	0.02
HG25	160	15	RPM-1000	Push	0.02
HG25	205	15	RPM-1000	Push	0.02
HG25	160	30	RPM-1000	Push	0.02
HG25	205	30	RPM-1000	Push	0.02
EG5 (5.5)	160	0	RPM-1000	Push	0.02
EG5 (5.5)	205	0	RPM-1000	Push	0.02
EG5 (5.5)	160	15	RPM-1000	Push	0.02
EG5 (5.5)	205	15	RPM-1000	Push	0.02
EG5 (5.5)	160	30	RPM-1000	Push	0.02
EG5 (5.5)	205	30	RPM-1000	Push	0.02
EG5 (3.0)	115	0	RPM-1000	Push	0.02
EG5 (3.0)	160	0	RPM-1000	Push	0.02
EG5 (3.0)	205	0	RPM-1000	Push	0.02
EG5 (3.0)	115	15	RPM-1000	Push	0.02
EG5 (3.0)	160	15	RPM-1000	Push	0.02
EG5 (3.0)	205	15	RPM-1000	Push	0.02
EG5 (3.0)	115	30	RPM-1000	Push	0.02
EG5 (3.0)	160	30	RPM-1000	Push	0.02
EG5 (3.0)	205	30	RPM-1000	Push	0.02

APPENDIX B
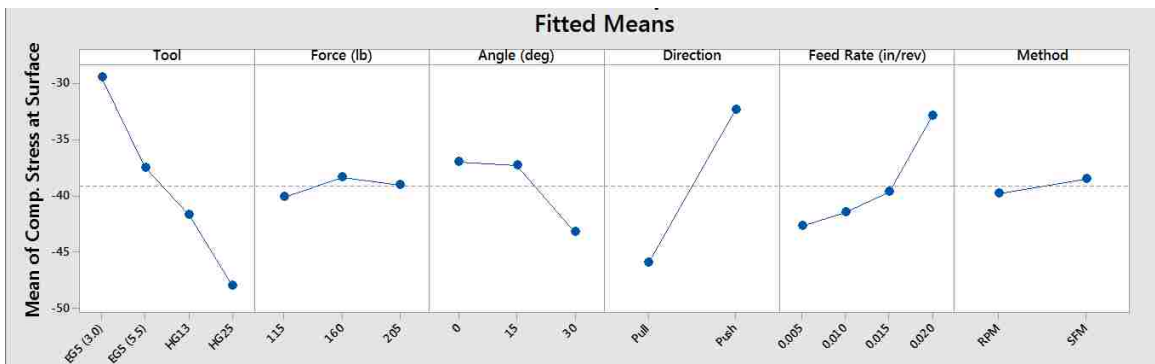
DOE 2 EXPERIMENTAL DESIGN

Tool	Force (lb.)	Angle (deg)	Control	Direction	Feed Rate (in/rev)
EG5 (3.0)	205	15	RPM-500	Push	0.005
EG5 (3.0)	205	15	RPM-500	Push	0.01
EG5 (3.0)	205	15	RPM-500	Push	0.015
EG5 (3.0)	205	15	RPM-500	Pull	0.005
EG5 (3.0)	205	15	RPM-500	Pull	0.01
EG5 (3.0)	205	15	RPM-500	Pull	0.015
EG5 (3.0)	205	15	RPM-1000	Push	0.005
EG5 (3.0)	205	15	RPM-1000	Push	0.01
EG5 (3.0)	205	15	RPM-1000	Push	0.015
EG5 (3.0)	205	15	RPM-1000	Pull	0.005
EG5 (3.0)	205	15	RPM-1000	Pull	0.01
EG5 (3.0)	205	15	RPM-1000	Pull	0.015
EG5 (3.0)	205	15	SFM-675	Push	0.005
EG5 (3.0)	205	15	SFM-675	Push	0.01
EG5 (3.0)	205	15	SFM-675	Push	0.015
EG5 (3.0)	205	15	SFM-675	Pull	0.005
EG5 (3.0)	205	15	SFM-675	Pull	0.01
EG5 (3.0)	205	15	SFM-675	Pull	0.015
EG5 (3.0)	205	15	SFM-1350	Push	0.005
EG5 (3.0)	205	15	SFM-1350	Push	0.01
EG5 (3.0)	205	15	SFM-1350	Push	0.015
EG5 (3.0)	205	15	SFM-1350	Pull	0.005
EG5 (3.0)	205	15	SFM-1350	Pull	0.01
EG5 (3.0)	205	15	SFM-1350	Pull	0.015

APPENDIX C

MAIN EFFECTS CHARTS OF THE GLOBAL ANOVA

Fitted Means (Mean of Principle Angle at Surface) — Tool, Force (lb), Angle (deg), Direction, Feed Rate (in/rev), Method

Fitted Means (Mean of Depth of Max. Comp. Stress) — Tool, Force (lb), Angle (deg), Direction, Feed Rate (in/rev), Method

Fitted Means (Mean of Max. Comp. Stress) — Tool, Force (lb), Angle (deg), Direction, Feed Rate (in/rev), Method

Fitted Means (Mean of Comp. Stress at Surface) — Tool, Force (lb), Angle (deg), Direction, Feed Rate (in/rev), Method

Fitted Means

BIBLIOGRAPHY

[1]   Abrão, A.m., et al. "The Influence of Deep Rolling on the Surface Integrity of AISI 1060 High Carbon Steel." *Procedia CIRP*, vol. 13, 2014, pp. 31–36., doi:10.1016/j.procir.2014.04.006.

[2]   Beghini, M., et al. "Experimental Parameter Sensitivity Analysis of Residual Stresses Induced by Deep Rolling on 7075-T6 Aluminum Alloy." *Surface and Coatings Technology*, vol. 254, 2014, pp. 175–186., doi:10.1016/j.surfcoat.2014.06.008.

[3]   Jinlong, Lv, et al. "Experimental Study of Corrosion Behavior for Burnished Aluminum Alloy by EWF, EBSD, EIS and Raman Spectra." *Applied Surface Science*, vol. 273, 2013, pp. 192–198., doi:10.1016/j.apsusc.2013.02.012.

[4]   Jinlong, Lv, et al. "Investigation of Microstructure and Corrosion Behavior of Burnished Aluminum Alloy by TEM, EWF, XPS and EIS Techniques." *Materials Research Bulletin*, vol. 83, 2016, pp. 148–154., doi:10.1016/j.materresbull.2016.05.013.

[5]   Leong, K.c., and S.w. Lye. "Thermal-Based Tool Sensor for Ball Burnishing." *Journal of Mechanical Working Technology*, vol. 20, 1989, pp. 121–128., doi:10.1016/0378-3804(89)90023-5.

[6]   Mahajan, Deepak, and Ravindra Tajane. "A Review on Ball Burnishing Process: IJSRP February 2013 Publication." *A Review on Ball Burnishing Process | IJSRP February 2013 Publication*, www.ijsrp.org/research-paper-0413.php?rp=P161004.

[7]   Majzoobi, G.h., et al. "The Effects of Deep Rolling and Shot Peening on Fretting Fatigue Resistance of Aluminum-7075-T6." *Materials Science and Engineering: A*, vol. 516, no. 1-2, 2009, pp. 235–247., doi:10.1016/j.msea.2009.03.020.

[8]   Mohseni, E., et al. "A Study on Surface Modification of Al7075-T6 Alloy against Fretting Fatigue Phenomenon." *Advances in Materials Science and Engineering*, vol. 2014, 2014, pp. 1–17., doi:10.1155/2014/474723.

[9]   Naidu, N, and S Raman. "Effect of Shot Blasting on Plain Fatigue and Fretting Fatigue Behaviour of Al?Mg?Si Alloy AA6061." *International Journal of Fatigue*, vol. 27, no. 3, 2005, pp. 323–331., doi:10.1016/j.ijfatigue.2004.07.007.

[10] Patel, P. N. "Parametric Optimization of Ball Burnishing Process Parameter for Hardness of Aluminum Alloy 6061." *IOSR Journal of Engineering*, vol. 4, no. 8, 2014, pp. 21–26., doi:10.9790/3021-04822126.

[11] Quran, Firas M. F. Al. "The Effect of Roller Burnishing on Surface Hardness and Roughness of Aluminum Alloy." *International Journal of Mechanics and Applications*, Scientific & Academic Publishing, article.sapub.org/10.5923.j.mechanics.20150502.02.html.

[12] Schajer, G. S. "Advances in Hole-Drilling Residual Stress Measurements." *Experimental Mechanics*, vol. 50, no. 2, 2009, pp. 159–168., doi:10.1007/s11340-009-9228-7.

[13] Schajer, Gary S. *Practical Residual Stress Measurement Methods*. Ch1. Wiley, 2013.

[14] Schajer, Gary S. *Practical Residual Stress Measurement Methods*. Ch2. Wiley, 2013.

[15] Stephens, Ralph Ivan. *Metal Fatigue in Engineering*. Wiley, 2001.

[16] "Tech Note TN-502." *Vishaypg.com*, Vishay Precision Group, 1 Nov. 2010, www.vishaypg.com/docs/11052/tn502.pdf.

[17] "Tech Note TN-503." Vishaypg.com, Vishay Precision Group, 1 Nov. 2010, www.vishaypg.com/docs/11053/tn503.pdf

[18] "Tech Note TN-507." *Vishaypg.com*, Vishay Precision Group, 1 Nov. 2010, www.vishaypg.com/docs/11057/tn5071.pdf

[19] Wagner, L. "Mechanical Surface Treatments on Titanium, Aluminum and Magnesium Alloys." *Materials Science and Engineering: A*, vol. 263, no. 2, 1999, pp. 210–216., doi:10.1016/s0921-5093(98)01168-x.

[20] Wong, Chow Cher, et al. "Deep Cold Rolling of Features on Aero-Engine Components." *Procedia CIRP*, vol. 13, 2014, pp. 350–354., doi:10.1016/j.procir.2014.04.059.

[21] Yan, B.h., et al. "Surface Modification of Al–Zn–Mg Alloy by Combined Electrical Discharge Machining with Ball Burnish Machining." *International Journal of Machine Tools and Manufacture*, vol. 42, no. 8, 2002, pp. 925–934., doi:10.1016/s0890-6955(02)00026-3.

[22] Zinn, W., and B. Scholtes. "Mechanical Surface Treatments of Lightweight Materials—Effects on Fatigue Strength and Near-Surface Microstructures." *Journal of Materials Engineering and Performance*, vol. 8, no. 2, 1999, pp. 145–151., doi:10.1361/105994999770346972.

VITA

Andrew Layer was born in 1992 in New Albany, Indiana to John and Katrina Layer. He received his bachelor of science degree in Mechanical Engineering from the Missouri University of Science and Technology in December 2014. He accepted a position of Product Engineer from Accuride Corporation and has continued advancing in this position to the present time. In 2017 Andrew was accepted into Missouri University of Science and Technology's distance education program to pursue a master of science degree in Mechanical Engineering. In December 2019, he received his master's degree in Mechanical Engineering from Missouri S&T.